# STATE-OF-THE-ART OF CONSTRUCTION STONES FOR MASONRY EXPOSED TO HIGH TEMPERATURES

Francesca Sciarretta[a]*, Javad Eslami[a], Anne-Lise Beaucour[a], Albert Noumowé[a]

[a]) Cergy Paris Université, Laboratoire de Mécanique des Matériaux du Génie Civil (L2MGC), 5 Mail Gay-Lussac, 95000 Neuville-sur-Oise, France

*) corresponding author

## ABSTRACT

The consequences of fires on cultural heritage building and monuments can be deleterious, as historic and recent cases demonstrate. In particular, devastating fires have ravaged stone masonry monuments, which must be properly repaired and retrofitted with rational, performance-based design. Updated quantitative knowledge and design tools – especially about materials' properties – is necessary to implement such performance-based strategies. Under this perspective, the paper takes into account a number of references to present a state-of-the-art about the current knowledge of high-temperature behaviour of different families of construction stones – namely granites, marbles, sandstones and limestones. The stones' strain behaviour, thermal properties (conductivity and specific heat) and mechanical properties (compressive strength, elastic modulus, peak compressive strain, Poisson's ratio and tensile strength) are accounted for. The residual mechanical properties, i. e. after high temperature exposure, are under particular consideration in view of evaluating the residual structural reliability of stone masonry structures after a fire with numerical methods. The micro- and macroscopic level are put into relationship, linking the information about the chemical and physical transformation of component minerals under high temperatures to the changes in the stones' properties and thermal strain. The aim is to provide quantitative information, namely mean values and intervals of confidence, for the considered properties to be appliable in the performance-based fire design and evaluation of stone masonry structures.

KEYWORDS: stone masonry, high temperatures, thermal properties, mechanical behaviour, thermal strain

## 1. INTRODUCTION

All over the world, masonry is the historic construction material *par excellence*. Historic masonry buildings are vulnerable to fire, due to wooden or metallic decks and roofs, typically high fire loads and frequent works of maintenance. In fact, many ancient buildings and monuments have withstood violent fires during their history; in fact, structural masonry often survives fires due to high structural stiffness and stabilizing mass. In such cases, the structural reliability of buildings must be granted, as a mandatory requirement for preservation, recover and historic-artistic safeguard of cultural heritage. On the other hand, the residual structural capacity of masonry walls, pillars, columns and vaults after fire is not easy to quantify, due to the high number of relevant parameters in modelling both masonry and fire [1, 2]. Of course, the residual structural capacity depends on the residual mechanical properties of the masonry components, namely the strength, elastic modulus and stress-strain behaviour; such properties are generally affected by the high temperature history, by means of chemical-physical transformation of the component minerals; as well, the effects of thermal expansion and/or contraction must be accounted for. Finally, the evolution of temperature distribution is in relationship with the thermal conductivity, specific heat and density of the materials.

The attention of research is high on cultural heritage at risk [3, 4]; currently, more interest is growing around the structural stability of stone masonry monuments attacked by fire. Especially in France, after the well-known fires of the cathedrals of Chartres, Notre Dame de Paris and Nantes, research is receiving new impulse to investigate the residual structural reliability of stone masonry monuments after fire. In particular, the National Agency for Research (ANR) is now funding two different projects of collaborative research aimed at advancing the scientific knowledge in this field. One of these is *POSTFIRE – Safety and preservation of cultural heritage stone masonry buildings after fire events*, a 4-years project of collaborative research among public and private institutions guided by the Cergy Paris University. POSTFIRE features extended experimental investigations from the material to the structural scale, aimed at setting up numerical models of masonry under pre-fire, fire and post-fire conditions, to be calibrated by the case study of the Notre Dame cathedral in Paris [5].

Heritage buildings have generally high fire loads, due to the presence of wooden members (structural and non-structural), decorations, tapestry, paper and furniture; from this point of view, libraries and archives are of particular concern. Hence, cellulosic fires are generally expected to develop in such structures. The spread rates can be initially slow, but after the ignition phase temperatures can quickly rise up to 1000-1200°C. Fire durations are strongly affected by the site's accessibility to firefighters and by the viable means of extinction. The use of water for fire quenching is of course expected; however, the heavy damage to the marbles of Chapel of the Holy Shroud in Turin, Italy (burnt in 1997 [6]), demonstrates the need of avoiding the thermal shock of hot stone masonry members, as far as it is possible. As well, the impact of hose stream, or water masses poured from above, can be dangerous to slender loadbearing members.

It is recognised that only the performance-based approach could be suitable for the fire performance assessment of cultural heritage buildings. Discontinuous and continuous approaches are usually applied to model stone masonry, e. g. [7, 8]. In fact, only methods and tools explicitly implementing the material properties into analytical calculations could be able to account for the peculiarities – materials, structural types, presence of different construction phases, etc. – of ancient buildings [9]. However, even performance-based codes for the fire resistance assessment of masonry structures – like Eurocode 6 [10] and NFPA 914 [11] – do not contain specific strength calculation methods for post-fire situation. To enable such methods, it is essential to establish relationships between temperatures and residual properties for a wide range of masonry materials. In the field of civil engineering, the high temperature behaviour of stones is much less known and investigated than that of concrete and clay-based masonry blocks. Generally, only destructive tests (DT) provide quantitative assessment of mechanical properties; but the need for preservation generally induces post-fire surveyors to rely mainly upon non-destructive tests (NDT) [12] or, if available, pre-existing data. Whenever possible, calibration between NDT and DT parameters maximises the knowledge increase, minimising the time, cost and impact of the survey [13].

The information collected in this paper refers to tests on small samples of materials tested in laboratory, with heating and cooling conditions reproduced in laboratory by means of muffles and furnaces. The material samples are small enough to reach uniform temperatures, and the temperature evolution is controlled. On the other hand, it must be noted that real fires feature temperature fluctuations in space and time, as well as possible direct contact with flame. However, the non-uniform exposure of masonry members in real fires is rarely taken into consideration in laboratory research, due to the non-repeatability of tests simulating a real fire exposure, as well as to difficult temperature measurement. A research by Mc Cabe et al. [14] points out that the deposit of soot due to the burning of wood creates a waterproof veneer which entraps salts and water, causing delayed disruption of stone; for this reason, stone blocks exposed to real fire simulation have a worse long-term residual behaviour than blocks exposed to high temperatures in laboratory. This aspect should be taken into consideration in post-fire reliability analyses of buildings attacked by fire. Moreover, masonry structures are generally massive; as well, the materials' low conductivity and possibly relevant content in water (which steeply increases the specific heat in the range 50-100°C) make the material's temperature-dependent decay not uniform through the depth of a masonry member.

The presence of mortar – in historic buildings, mostly hydrated aerial lime mortars, obtained by adding pozzolanic materials to the mix – as a component of masonry also deserves attention in thermal and thermal-mechanical modelling. Literature about the thermal, thermal-mechanical and fire behaviour of lime-based mortars is not abundant [15, 16]; the below considerations about limestones (Sections 2 to 4) can be useful to understand the behaviour of lime-based mortars. As well, information about sandstones and granites can apply to siliceous sand and fine aggregate.

Structural models should appropriately account for the possible presence of metallic elements (iron, cast iron or steel). Ties can connect multiple layers of a masonry members, or can collaborate to the load-bearing function within the masonry, e. g. counterbalance horizontal thrust. Unprotected steel elements lose their effectiveness in a sudden way once they reach the critical temperature (around 700°C). Attention must also be paid to the steel's elastic thermal expansion – the case of the Frauenkirche in Dresden, Germany, showed that the structural collapse was originated by the mismatch between the residual thermal strain of the stone pillars and the re-contraction of steel suspended walkways after fire [17].

Finally, the load level of compressive masonry members must be properly taken into account in fire structural analysis and assessment of residual reliability, especially for slender members. A high compressive load can have a dual effect under fire conditions. In fact, if the member is not free to expand, the vertical compressive stress provides a mechanical constraint to the tensile thermal strain, lowering the thermally-induced stress. However, for long fire durations, the structural geometry is modified by the thermally-induced displacement of slender members, as well as by significant portions of cross-sections becoming ineffective due to heat-induced material damage. In such cases, a P-Δ effect is triggered and the masonry member may collapse under the compressive load [18].

The paper's aim is to provide a state-of-the-art of the relevant thermal and mechanical properties of selected construction stones after high temperature exposure. It will enlighten the potential of available data and future research needs. Limestone and sandstone are very common types in structural parts of historic stone masonry [19-21]; marbles are used for precious decorations, fine claddings and pavements [22]; granites are also frequently used for external claddings, as well as for load-bearing masonry in some geographical areas [23]. From the macroscopic point of view, the geological origin of a territory marks the abundance of certain types of rocks. However, different species of a same rock type, with different porosity and strength, can be found in the same extraction zone (e. g. sandstones S6 and S7 in the following Sections). To understand the changes in properties, Section 2 describes the effect of stones' mineralogy and structure on the high temperature behaviour, especially the thermal dilatation. Section 3 presents the material properties measured under high temperatures (conductivity and specific heat). Section 4 displays the information about the mechanical properties of construction stones after high temperature exposure. Sections 2, 3 and 4 also contain graphs of mean values and 65% confidence intervals of normalised properties (i. e. thermal strain, conductivity, specific heat and mechanical properties), as a quantitative evaluation of the parameters as functions of temperature; they are calculated at temperature levels for which three or more data are available, without any extrapolation. Finally, Section 5 presents the effects of porosity, water content, anisotropy and features of thermal stress history on the thermal and mechanical properties. The paper's Appendix reports the features of all the materials accounted for, into tables A1 to A4 (data series G for granites, M for marbles, S for

sandstones and L for limestones); Tables A5 and A6 list the parameters and features of tests and Tables A7 to A10 the calculated mean values and 65-quantiles.


## 2. TEMPERATURE-DEPENDENT ALTERATIONS OF CONSTRUCTION STONES

The mineralogical phase changes induced by increasing (and then decreasing) temperatures entail mass loss and endo- or exothermal reactions within the constituent minerals of rocks. High-temperature exposure can also produce colour changes in stones; in fact, some minerals exhibit a colour change associated to a phase transformation. This is the basis of the non-destructive method of evaluation by colorimetric analysis, aimed at identifying the highest temperature experienced by a stone based on the colour retained after exposure [23, 24]. In the following subsections, the description is limited to the main minerals to be encountered throughout Sections 3 and 4.

Granites are igneous rocks containing a high percentage of feldspars, mainly potash feldspar and albite-oligoclase, quartz (>10%) and mafic minerals (amphibole, biotite or both, <10%). Granites are generally medium- to coarse-grained. Marbles are metamorphic rocks composed by carbonates, mainly calcite, dolomite or both. Limestones are sedimentary rocks composed by carbonates (>50%, mainly calcite), widely variable in texture and composition; fossil fragments are commonly present. Sandstones are sedimentary rocks composed by grain particles of sand size (consisting of quartz, feldspar and clay minerals), bound together by different types and amounts of cement [25].

### 2.1. Physical-chemical transformations of component minerals under high temperatures

Figure 1 shows the main temperature-induced phase transformations for silicates, carbonates and gypsum (the latter is a very common component of historic plasters), according to the tests performed by Sippel et al. [26]. Physical-chemical transformations can be opportunely observed in real time by combining two types of measurement [20], i. e. differential scanning calorimetry (DSC) and thermogravimetric analysis (TGA). In detail, DSC provides the variation of specific thermal flux per mass unit (mW/mg), enlightening peaks corresponding to endo- or exothermal reactions triggered by transformations; then, TGA puts out the per cent mass values at varying temperatures. Finally, X-ray diffraction images can provide insight of a rock's mineral composition, which can change due to the heating and subsequent cooling process.

At high temperatures, phyllosilicates and clay minerals (e. g. chlorite, biotite or illite) undergo dehydroxilation, originating the release of Fe+ ions; the latter generally oxidate and form hematite ($Fe_2O_3$), as enlightened by investigations with X-ray diffraction [27]. Dehydroxilation usually develops until 800°C and may begin at different temperatures, e. g. 200°C for biotite, 300°C for limonite, 400°C for kaolinite, 500°C for masonite, whose dehydroxilation can last over 800°C (dashed pieces of arrow in Figure 1). Silica ($SiO_2$) is present in rocks as quartz, at atmospheric pressure conditions; in particular, it takes the form of quartz-$\alpha$ up to 573°C, and then of quartz-$\beta$ until 870°C. This phase

change at increasing temperature is reversible and associated to a shape change of the crystalline lattice, i. e. from rhombohedral to hexagonal system. The switch can be identified, in rocks with significant amounts of quartz (>5%), by a feeble endothermal peak and slight mass loss [28].
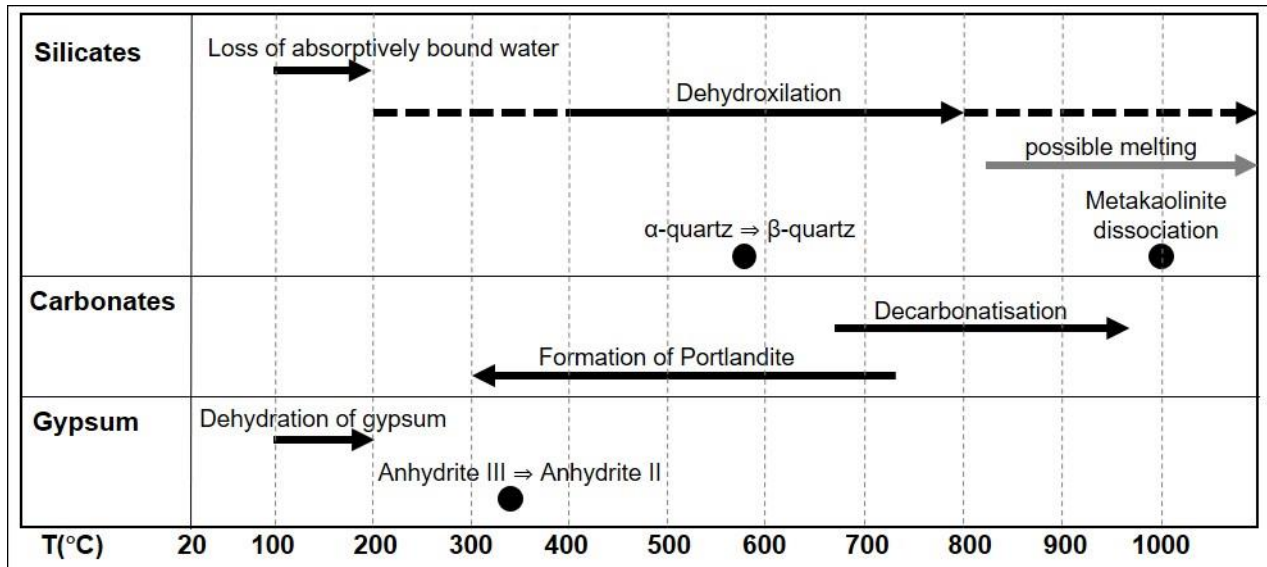


**Figure 1.** Main temperature-induced transformations of minerals [26] (the dashed pieces of arrow mark the possible range of occurrence)

Calcite (calcium carbonate, $CaCO_3$) and dolomite (calcium and magnesium carbonate, $CaMg(CO_3)_2$) are subject to decarbonisation under high temperatures, encountering a mass loss of about 44% (for calcite) or 45% (for dolomite) at the end of the process, i. e. around 900°C [29]. The mass loss of a calcareous stone is directly proportional to its content in calcite, according to TGA measurements [30]. Calcite is chemically stable up to 700°C circa; at such temperature, decarbonation, marked by a clear endothermal peak in TGA, turns calcium carbonate into carbon dioxide and quicklime. Then the latter (CaO), in contact with water during cooling, forms portlandite, i. e. $Ca(OH)_2$, according to the stoichiometric formulas in Equations (1) and (2). The re-hydration of quicklime is related to volume increase, eventually leading even to macroscopic cracking [19].

$$CaCO_3 \rightarrow CaO + CO_2 \qquad (1)$$

$$CaO + H_2O \rightarrow Ca(OH)_2 \qquad (2)$$

The decarbonation of dolomite starts around 650°C and presents a TGA peak, which occurs a little earlier than the decomposition of calcite [28]. The resulting periclasium (magnesium oxide) gets in combination with water and forms brucite, i. e. $Mg(OH)_2$, according to Equations (3) and (4).

$$CaMg(CO_3)_2 \rightarrow MgO + CO_2 + CaCO_3 \rightarrow MgO + CaO + 2\ CO_2 \qquad (3)$$

$$MgO + H_2O \rightarrow Mg(OH)_2 \qquad (4)$$

Finally, gypsum-bearing sulphate rocks undergo gypsum dehydration up to anhydrite III ($CaSO_4$) between 100 and 200°C, and then to anhydrite II with an exothermal reaction around 330°C. Within this temperature range, dehydration can give a significant contribution to the thermal inertia of a masonry element protected by e. g. a layer of gypsum-based plaster.

## 2.2. Colour changes associated to physical-chemical transformations under high temperatures

The formation of hematite after dehydroxilation of clay minerals contained in a rock is at the origin of the rubefaction phenomenon, that is a visible turn to pink, red or brownish red [23, 31]. In sandstones, colour changes almost correspond to the effect of dehydroxilation [32]; in brown or buff coloured sandstones, rubefaction may not be apparent until 400°C [33], but it can persist even up to 1000°C [19]. Brown or buff coloured limestones become pink or reddish brown, and more reddish from 400°C on, while light coloured limestones can turn to pink around 400°C [19]. Some greenish minerals show peculiar changes, e. g. glauconite turns to brownish at 450°C and dark brownish at 900°C, when hematite starts forming up; chlorite changes from pale green to brownish at 300°C and then to yellowish at 900°C. Such individual colour changes are often hidden by the reddening of other iron-bearing minerals [27]. Finally, colour changes due to hydroxylation have no uniform trends, in particular the darkening of an iron-bearing stone is not a strict consequence of heating, and it is not directly related to the experienced temperature [27]. Moreover, darkening due to physical-chemical transformations under high temperatures must be distinguished from effects of weathering [34].
Pure calcite rocks (e. g. marbles or travertines) are greyish around 600°C, and further revert to white, due to the formation of CaO, but losing the original translucence of crystals [35]. Thus, calcite-bearing stones show a two-phase colour change, i. e. darkening at the beginning of decarbonatation, followed by a dull white coloration from 800°C on. On the other hand, a grey colour at about 500°C can also appear due to charring of traces of organic matter, which are often undetectable by analysis. This can overshadow other colour changes, but carbon traces vanish at higher temperatures [32].

## 2.3. Thermal expansion of stones depending on the nature of component minerals

Thermal expansion is characterised by two parameters, i. e. the coefficient of linear thermal expansion $\alpha$ (usually expressed in °C$^{-1}$) expressing the variation of length (mm/m) through the temperature interval, and the residual thermally-induced strain $\varepsilon_r$ which comes from microcrack development and/or growth of pre-existing microcrack state, after heating and subsequent cooling. A temperature increase entails thermal strain development within a stone, through the dilatation (or contraction) of the component minerals. The presence of minerals having thermal dilatations of different magnitude, and their anisotropic thermal expansion due to layering, is thus at the origin of differential dilatations. Generally, the linear thermal expansion coefficient (Table 1) varies with temperature and direction, with respect to the crystalline axis (c-axis) [36-38].

**Table 1.** Linear thermal expansion of some rock-forming minerals

| Mineral | Ref. | Temperatures (°C) | Linear thermal expansion coefficient (°C$^{-1}$) | |
|---|---|---|---|---|
| | | | **Parallel to c-axis** | **Perpendicular to c-axis** |
| Quartz | [36] | 0-80 | $7.7 \times 10^{-6}$ | $13.3 \times 10^{-6}$ |
| | [37] | 40 | $7.81 \times 10^{-6}$ | $14.19 \times 10^{-6}$ |
| | | 100 | $8.4 \times 10^{-6}$ | $15.4 \times 10^{-6}$ |
| | | 200 | $9.0 \times 10^{-6}$ | $17.6 \times 10^{-6}$ |
| | | 400 | $14.2 \times 10^{-6}$ | $27.2 \times 10^{-6}$ |
| | | 573 | $92.0 \times 10^{-6}$ | $191.6 \times 10^{-6}$ |
| | | >573 | $-3.2 \times 10^{-6}$ | $-5.8 \times 10^{-6}$ |
| Calcite | [36] | 0-85 | $25.1 \times 10^{-6}$ | $-5.6 \times 10^{-6}$ |
| | [38] | 675 | $31.6 \times 10^{-6}$ | $-1.25 \times 10^{-6}$ |
| | | 700 | $31.9 \times 10^{-6}$ | $-1.68 \times 10^{-6}$ |
| | | 750 | $33.7 \times 10^{-6}$ | $-2.24 \times 10^{-6}$ |
| | | 800 | $37.3 \times 10^{-6}$ | $-2.38 \times 10^{-6}$ |
| Dolomite | [36] | 24-700 | $25.8 \times 10^{-6}$ | $6.2 \times 10^{-6}$ |

Quartz has a remarkably anisotropic thermal dilatation, with strains about twice as high along the perpendicular to the c-axis; moreover, thermal expansion grows until the phase change at 573°C, then the strain stabilises. Calcite, besides anisotropy, shows dilatation along the c-axis and contraction along the perpendicular direction, so that, at 600°C the strains are respectively 2% and –0.22% [39]. Thus, the differential dilatation often leads calcite-bearing rocks to granular decohesion. Dolomite, despite anisotropy, expands along both directions and is less sensitive than calcite to thermal cycles. Experimental information about the macroscopic effects of rocks' anisotropy on the thermal and mechanical properties is reported in Section 5. Other factors are also crucial in the entity and consequences of thermal expansion. Rocks with similarities in mineralogical composition can show linear thermal strains of different magnitude [40], due to the texture and grain size; in fact, the thermal dilatation is greater for larger grain size, and heterogeneous textures offer more allowance. Fine-grained anisotropic limestones expand more in parallel than perpendicular direction to the bedding; while coarse-grained show the opposite behaviour [41]. Finally, also a rock's initial porosity affects its ability to accommodate thermal strain; in fact, rocks of lower initial porosity (e. g. like in marbles) can develop micro-cracks at relatively low temperatures [42], while porous stones allow for less constrained dilatation [26]. The data proposed in Figure 2A-D regard selected materials from the considered sources [25, 26, 43-46]. The data are generally obtained with dilatometric tests on samples of variable size, as reported in Table A5 in the Appendix. A picture of a typical dilatometric apparatus is shown in Figure 3.

From Figure 2, the trends of the thermal strain behaviour are clear. As expected, similarities can be noticed between granites (Figure 2A) and sandstones (Figure 2C), containing silicates, and between marbles (Figure 2B) and limestones (Figure 2D), which are rich in carbonates. However, the strain increase of sandstones stops after the transition point of quartz at 573°C, while it continues in granites; the strain reversal of limestones after 800-900°C is not enough substantiated in marbles, possibly due to the scarcity of data. The higher values for granites than for sandstones, beyond 600°C, may be due to the lower porosity; the same holds for marbles, in comparison with limestones.
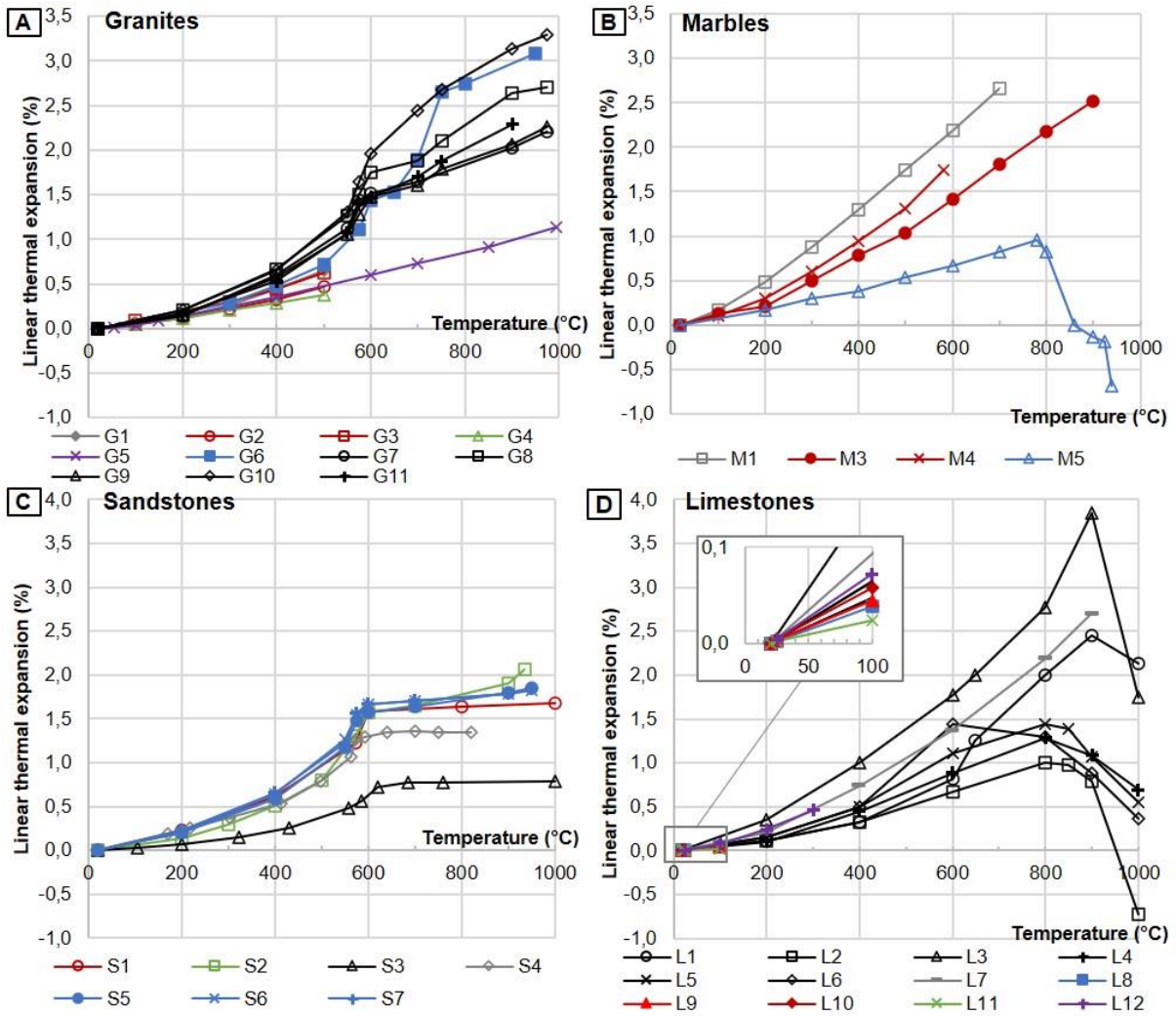
**Figure 2.** Thermal strain of granites (A), marbles (B), sandstones (C) and limestones (D)
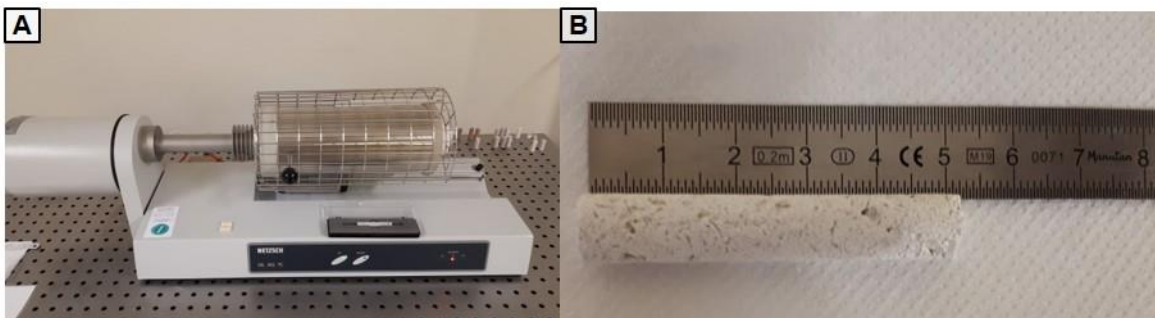


**Figure 3.** Dilatometer for thermal strain measurement (A) and stone sample (B) [43]

The interaction of exposure conditions (heating rate, maximum temperature, and cooling regime) and intrinsic features of the materials (mineralogy, porosity, initial cracking state, texture and granularity) generally leads to residual strain ($\varepsilon_r$). Since it gives a quantitative measure of the post-exposure crack development intensity, $\varepsilon_r$ is the main parameter related to a stone type's thermal sensitivity. Table 2 lists values of $\varepsilon_r$ for different types of constructions stones [26, 45, 46]; values at

lower temperatures (80-90°C) can also be found in literature, e. g. [47, 48]. The effects of anisotropy, which are of course relevant for the thermal strain, are treated in detail in Section 5.

**Table 2.** Maximum and residual strain of selected rocks after heating at target temperatures

| Stone type | Porosity (%) | Temperature (°C) | Maximum strain (%) | Residual strain (%) |
|---|---|---|---|---|
| Granite, Germany [26] | 0.11 | 500 | 0.76 | 0.20 |
| | | 700 | 1.94 | 0.94 |
| | | 950 | 3.09 | 2.77 |
| Calcite marble, Italy [26] | 0.21 | 500 | 1.03 | 0.54 |
| | | 950 | 2.52 | -2.67 |
| Pure calcite marble, Italy [26] | 0.26 | 580 | 1.74 | 0.95 |
| Dolomite marble, Greece | 0.54 | 580 | 0.70 | 0.21 |
| | | 950 | -0.69 | -1.79 |
| Limestone, Germany [26] | 4.64 | 950 | 2.45 | -0.68 |
| Limestone, Massangis, France [43] | 11.2 | 500 | 0.58 | 0.21 |
| | | 750 | 1.70 | 1.00 |
| | | 1050 | 2.20 | 0.81 |
| Limestone, Lens, France [43] | 15.4 | 500 | 0.41 | 0.17 |
| | | 750 | 0.64 | 0.27 |
| | | 1050 | -0.62 | -2.90 |
| Limestone, Euville, France [43] | 17.2 | 500 | 1.02 | 1.12 |
| | | 750 | 1.60 | 2.01 |
| | | 1050 | 0.70 | -0.92 |
| Limestone, Migné, France [43] | 26.8 | 500 | 0.76 | 0.19 |
| | | 750 | 1.33 | 0.51 |
| | | 1050 | 0.33 | -1.23 |
| Limestone, St. Maximin, France [43] | 29.7 | 500 | 0.88 | 0.34 |
| | | 750 | 1.45 | 0.61 |
| | | 1050 | 1.00 | -0.39 |
| Limestone, Savonnières, France [43] | 30.7 | 500 | 0.66 | 0.27 |
| | | 750 | 1.05 | 0.45 |
| | | 1050 | 0.00 | -1.75 |
| Grey sandstone, Germany [26] | 4.41 | 500 | N/A | 0.55 |
| | | 950 | N/A | 1.44 |
| Red sandstone, Germany [26] | 5.33 | 500 | 0.80 | 0.00 |
| | | 950 | 2.26 | 1.65 |
| Calcitic sandstone, Germany [26] | 6.59 | 500 | N/A | 0.30 |
| | | 950 | N/A | 2.52 |
| Yellow sandstone, Germany [26] | 16.68 | 950 | N/A | 0.43 |

The transition of quartz at 573°C entails a sudden and remarkable expansion. Although the transformation reverts with cooling, very high residual strains can be observed in quartz-bearing stones heated beyond the transition point, because of intergranular microfractures within quartz grains. The progressive fracture process can be one-stage, with a single strain discontinuity around 573°C, or two-stage with a further ramp after 700°C, as found out by Sippel [26]. Generally, the higher is the coefficient of thermal expansion, the higher the residual strain; however, a high initial porosity (>15%) can very much attenuate the residual strain of silicate rocks even after heating up to 950°C and subsequent cooling (Table 2, last row).

As far as it concerns calcareous stones, decarbonatisation produces a noticeable contraction (negative residual strain) after heating beyond 800°C. Calcite marbles have high expansion coefficients and develop residual strains much higher than quartz-bearing stones, and even under 100°C [49]. This peculiarity can induce cracking and disintegration even before the start of decarbonatisation. On the other hand, dolomite marbles can be much less thermally sensitive [41],

showing very limited thermal strains even after a 600°C exposure [26]. Moreover, calcite-bearing stones usually show anisotropic thermal expansion (see Table 1 above and Section 5 below). Finally, carbonate rocks develop phase changes even during cooling, i. e. the formation of portlandite; after the end of the heating-cooling cycle, portlandite causes significant volume increase and cracking. In this way, high temperature exposure produces delayed effects, which can be deleterious and need to be taken into consideration [26, 27].

Figure 4 presents the mean values and 65% confidence intervals of the normalised coefficient of thermal expansion (i. e. the ratio of $\alpha_T$ as a function of temperature $T$, to the value $\alpha$ for the lowest measured $\Delta T$) in the 0-1000°C range, calculated for all the series plotted in Figure 2 without interpolations. The points of the mean line and the intervals are determined at each temperature for which at least values are available; only the parallel direction to the bedding plane is considered.
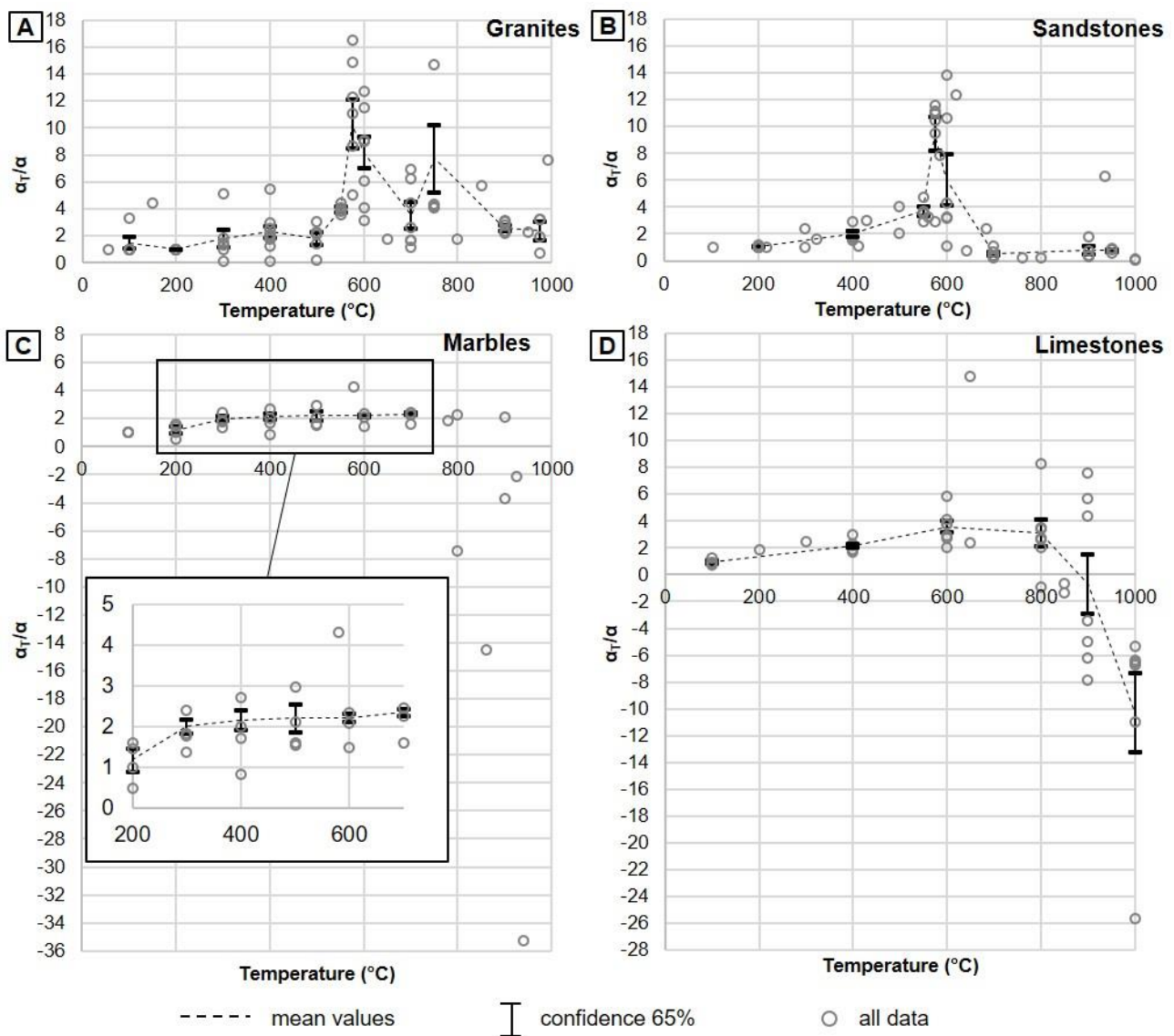


**Figure 4.** Mean values and 65-quantiles of normalised thermal expansion coefficient for A) granites, B) sandstones, C) marbles and D) limestones

According to Figures 4A-B, the peak corresponding to the quartz inversion at 573°C entails 8-10 times higher thermal expansion, considering the mean values, for quartz-rich stones. In the same Figures, the wide intervals of 65% confidence at the peaks indicate that the entity of increases in $\alpha_T$ can be very variable. Marbles (Figure 4C) show the lowest increase and very narrow intervals of confidence between 200 and 700°C, based on a good amount of data at relatively short steps of temperature (100°C). Limestones (Figure 4D) show a similar behaviour between 100 and 600°C, but with lesser data in the 100-400°C range and no data at all in the 400-600°C range. Generally, for all the four types of construction stones, the values are well compacted around the mean at least until 400°C. For granites and sandstones, even values at 900-1000°C have a good level of confidence.

## 3. THERMAL PROPERTIES OF CONSTRUCTION STONES AT HIGH TEMPERATURES

Generally, a material's thermal properties – namely conductivity $\lambda$ and specific heat $c_p$ – relate to its composition and microstructure. In fact, minerals of the same type and even of the same composition can show different values of thermal properties (Table 3, [50]). Other collections of values can be found in [51, 52]. Moreover, rocks with crystalline structure show faster conduction than amorphous and vitreous rocks of the same composition [53]; for instance, the different conductivity of silica minerals can be observed in Table 3. Besides experimental determination, the thermal properties of rocks can also be calculated from the type, quantity and thermal properties of component minerals, following very simple models; the values should account for porosity $\phi$, which also affects the thermal properties of rocks in a significant way, as a sort of thermal impedance [51].

**Table 3.** Conductivity at room temperature and specific heat at 0°C of rock-forming minerals [50]

| Mineral | | Formula | $\lambda$ (W/mK) | $c_P$ (J/kgK) |
|---|---|---|---|---|
| Carbonates | Calcite | $CaCO_3$ | 3.57 | 793 |
| | Aragonite | $CaCO_3$ | 2.23 | 780 |
| | Dolomite | $CaMg(CO_3)_2$ | 5.50 | 930 (at 60°C) |
| | Magnesite | $CaCO_3$ | 5.83 | 864 |
| Sulphates | Anhydrite | $CaSO_4$ | 4.76 | 520 |
| | Barite | $BaSO_4$ | 1.33 | 450 |
| Sulfides | Pyrite | $FeS_2$ | 19.20 | 500 |
| | Galena | $PbS$ | 2.28 | 207 |
| Hydroxides | Goethite | $\alpha\text{-}FeO \cdot OH$ | 2.91 | - |
| | Gibbsite | $Al(OH)_3$ | 2.60 | - |
| Oxides | Haematite | $\alpha\text{-}Fe_2O_3$ | 11.30 | 610 |
| | Magnetite | $Fe_3O_4$ | 5.10 | 600 |
| Silica minerals | Quartz | $\alpha\text{-}SiO_2$ | 7.69 | 698 |
| | Flint | $SiO_2$ | 3.71 | - |
| | Vitreous silica | $SiO_2$ | 1.36 | 700 |
| Phyllosilicates | Muscovite | $KAl_2(AlSi_3O_{10})(OH)_2$ | 2.32 | - |
| | Biotite | $K(Mg;Fe)(AlSi_3O_{10})(OH)_2$ | 1.17 | - |
| | Chlorite | $Mg_5AlSi_3O_{10}(OH)_8$ | 5.14 | - |
| Alkali-feldspar | Microcline | $KAlSi_3O_8$ | 2.49 | 680 |
| | Orthoclase | $KAlSi_3O_8$ | 2.31 | 610 |
| Plagioclase | Albite (Ab) 99%, anorthite (An) 1% | $Ab_{99}An_1$ | 2.31 | 709 |
| | Albite (Ab) 4%, anorthite (An) 96% | $Ab_4An_{96}$ | 1.68 | 700 |

Subsections 3.1 and 3.2 collect values of temperature-dependent $\lambda$ and $c_p$; Table A5 in the Appendix reports details of sample size and testing methods, if available. Figure 5 illustrates a typical apparatus for the measurement of thermal properties (Hotdisk TPL 1500 device [43]).
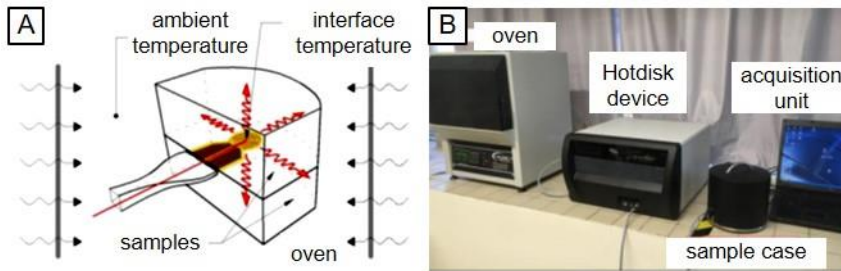


**Figure 5.** Hotdisk TPL 1500 device: thermocouple insertion (A) and equipment view (B) [43]

## 3.1. Thermal conductivity $\lambda$ as a function of temperature

Data for thermal conductivity as a function of temperature are presented for granites, marbles, sandstones and limestones (Figure 6A to 6D).
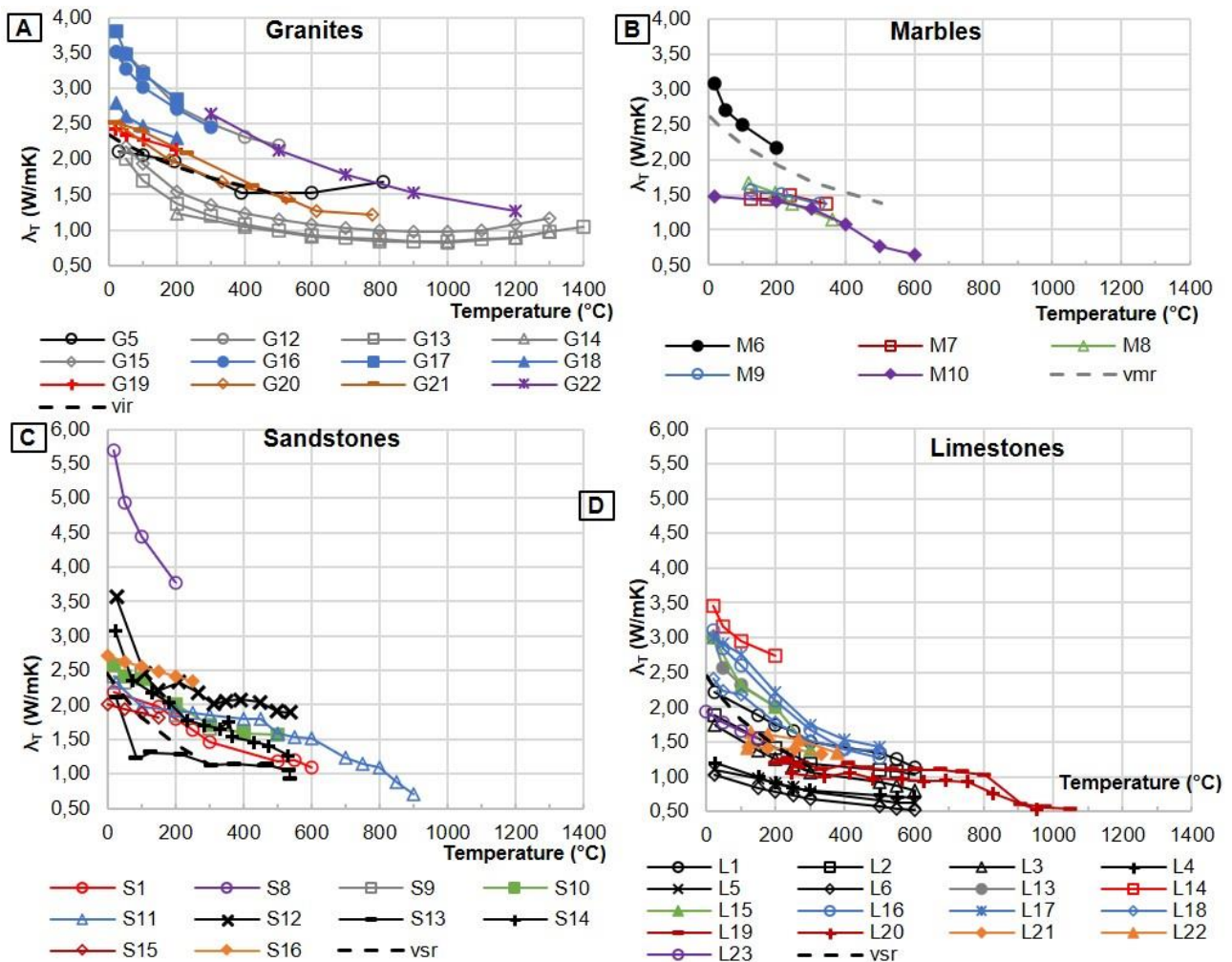


**Figure 6.** Thermal conductivity of granites (A), marbles (B), sandstones (C) and limestones (D) under high temperatures [20, 25, 44, 50, 54-58]

A good amount of information is available for granites, sandstones and especially limestones, while few data – and for a limited temperature range – refer to marbles. From a general point of view, the conductivity of stones decreases at increasing temperature – any increase is of negligible size – inducing slower heat transmission. The decrease is more rapid for higher initial conductivity, and is generally steeper in the 20-200°C range. It can be noticed that the curves labelled *vir*, *vmr* and *vsr*, corresponding to averages of various igneous, metamorphic and sedimentary rocks (Tables A1 to A4 in the Appendix) fit well into the envelope of the other curves.

The $\lambda_T$-*T* relation can be expressed by Equation 5 for most types of rocks up to 600°C [50, 52].

$$\lambda_T = \frac{1}{A+BT} \tag{5}$$

In some cases, e. g. some granites and sandstones (Figure 6A and 6C), the decrease reduces and can also revert beyond 600-800°C, due to the effect of rock-forming quartz [51]; in feldspar-rich stones, the thermal conductivity can be assumed as not depending from temperature [50]. It must be underlined that a rock's thermal conductivity is mostly affected by the porosity; research show very good correlations between the two parameters. Additional information is provided in subsection 5.1. Figure 7 presents the mean values and 65% intervals of confidence for the normalised thermal conductivity $\lambda_T/\lambda$, i. e. the ratio of the conductivity at temperature *T* to the value at the lowest temperature. Granites (Figure 7A) show a clear declining behaviour at least until 500°C; data for marbles (Figure 7B), being very few and disperse, do not allow establishing any line of mean values. The abundant data about sandstones (Figure 7C) have nonetheless a not negligible dispersion; for limestones (Figure 7D), the confidence of data is generally good up to 600°C. Generally, all the four graphs indicate the constant decline of thermal conductivity up to 400°C; then, up to 600°C, the parameter stabilises. At higher temperatures, data are too few to get any quantitative evaluation.
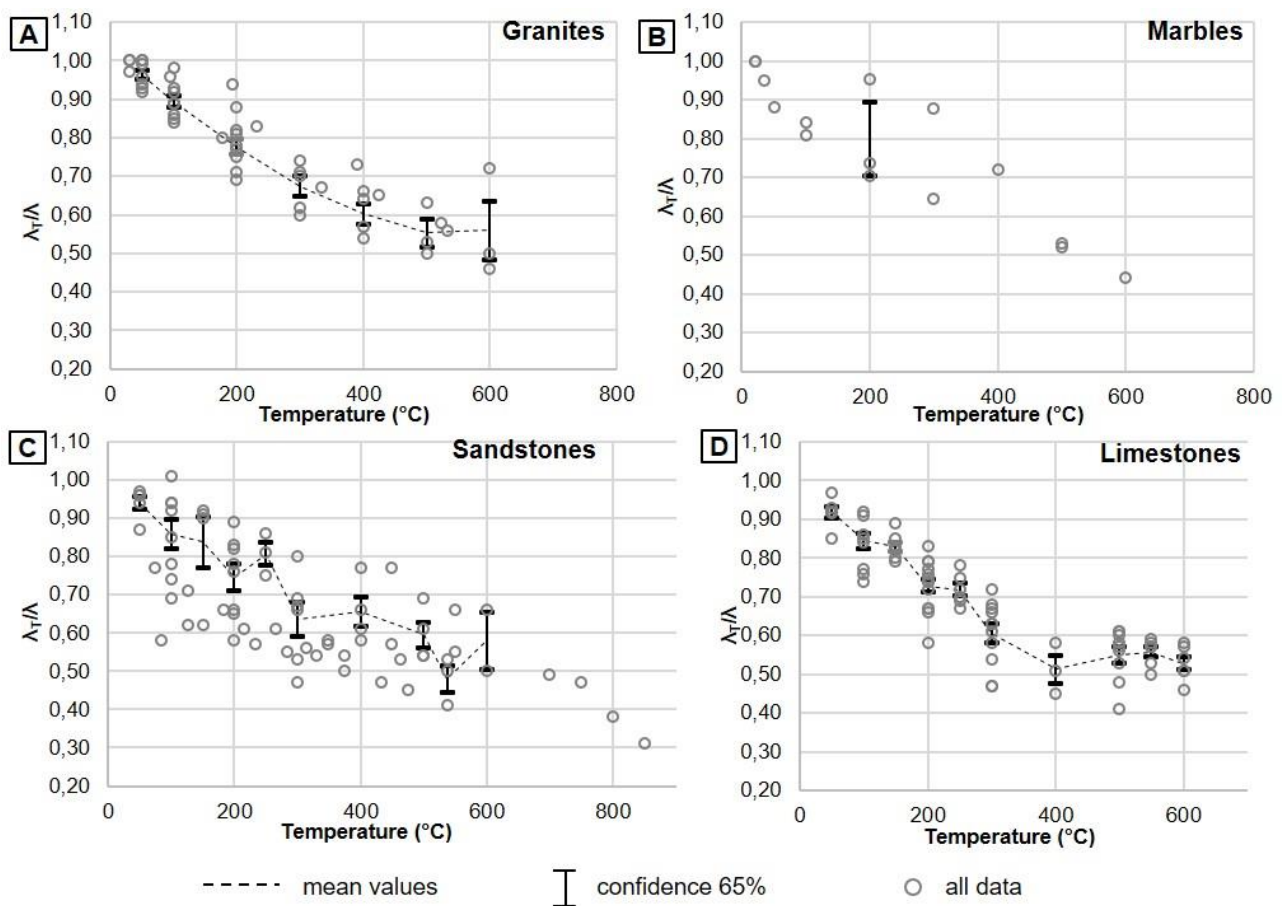
**Figure 7.** Mean values and 65-quantiles of normalised thermal conductivity for A) granites, B) sandstones, C) marbles and D) limestones [25, 43, 44, 50, 54, 55, 57, 58, 61]

## 3.2.  Specific heat $c_p$ as a function of temperature

The input of specific heat $c_p$ is required for transient thermal analyses; $c_p$ generally increases at increasing temperature, and the water content could affect its temperature-dependent evolution in the 0-200°C range [44]. Other reactions (e. g. the quartz transition) generating a significant amount of heat can bring on discontinuities in the $c_p$-$T$ curve. Eurocodes 2 and 6, for instance, account for the effect of water evaporation in the $c_p$-$T$ curves proposed for concrete and masonry [10, 59].

Figure 8 displays the $c_p$-$T$ graphs of granites (Figure 8A), marbles (Figure 8B), sandstones (Figure 8C) and limestones (Figure 8D) from the considered references. The effect of quartz transition is very clear, for instance, in granite G27 and sandstone S11, while peaks due to water evaporation appear between 100 and 200°C for sandstone S11 and marble M10. G22 [54], M10 [61] and S11 [56] show declining behaviour especially after 400°C; this contrasts the generally increasing trends of $c_p$-$T$ curves. The authors have attributed this contrasting trend to the heat-induced changes in the internal structure of sedimentary rocks, in particular enlightening the analogous behaviour of internal friction [56].
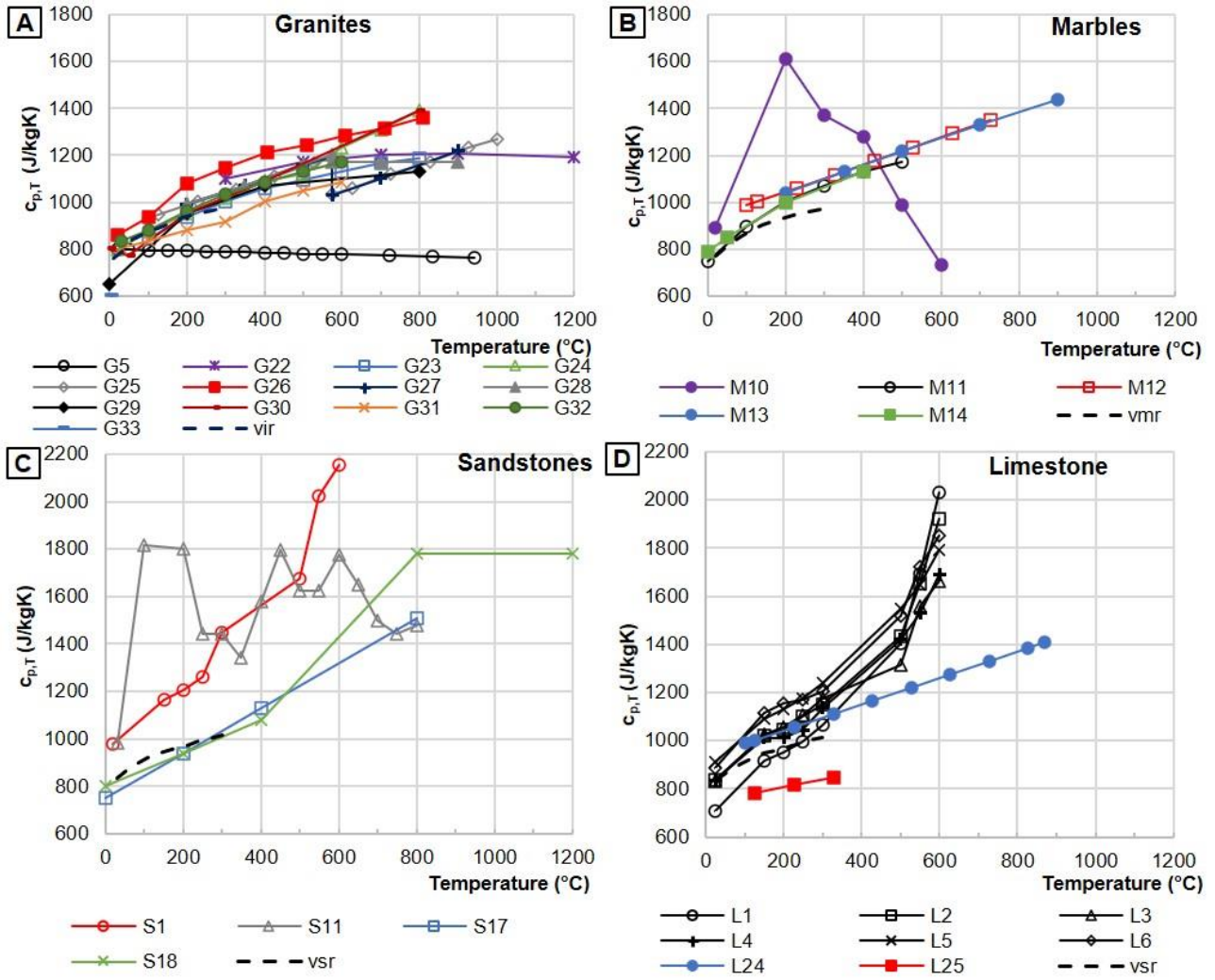
15

**Figure 8.** Specific heat of granites (A), marbles (B), sandstones (C) and limestones (D) under high temperatures [20, 25, 44, 50, 51, 54-56, 60, 61]

The specific heat of a rock can also be calculated from its constituents' specific heat values and their respective volumetric or weight fractions, at any temperature, according to the model of Equation 6; the calculated $c_p$-$T$ curves can be very accurate [51].

$$c_p = \sum_{i=1}^{n} \left( c_{p,i} \cdot \frac{x_i}{\rho_i} \right) \tag{6}$$

In Equation 6, $c_{p,i}$ is the specific heat per weight unit (J/kgK) of the $i$-th component mineral, $x_i$ is its decimal weight fraction and $\rho_i$ its density.

Figure 9 presents the mean values and 65% intervals of confidence for the normalised specific heat $c_{p,T}/c_p$. Granites (Figure 9A) and limestones (Figure 9D) show a good number of data and good enough confidence up to 300°C, while marbles (Figure 9B) and sandstones (Figure 9C) exhibit more disperse data. Generally, the growing trend of specific heat with temperature is fair enough for granites, sandstones and limestones. However, data are scarce and disperse for sandstones in the

range 400-800°C, and completely missing for limestones in the 300-500°C range. Finally, the scarcity of data on marbles does not allow defining a trend over a significant range of temperatures.
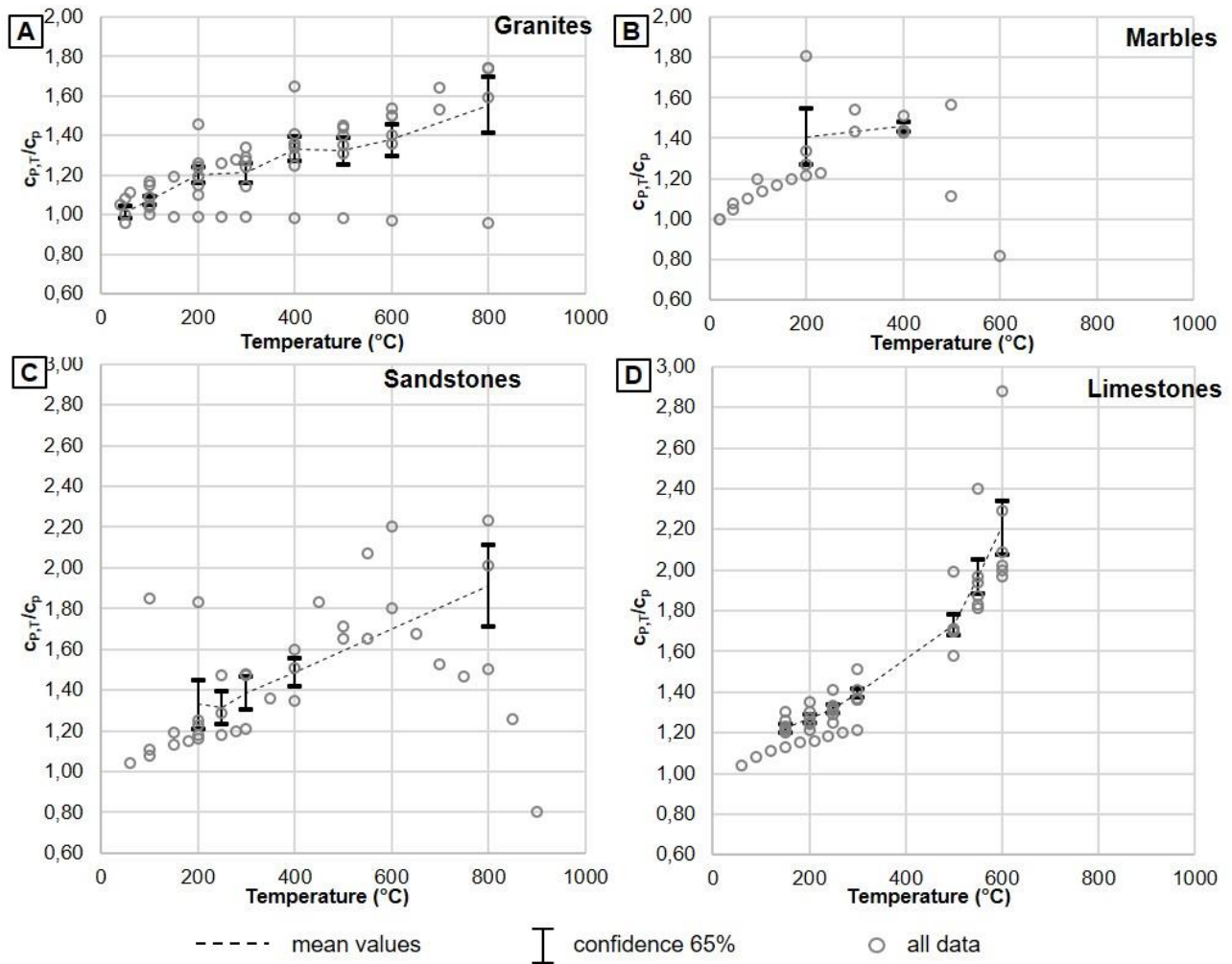


**Figure 9.** Mean values and 65-quantiles of normalised specific heat for A) granites, B) sandstones, C) marbles and D) limestones

## 4. MECHANICAL PROPERTIES OF CONSTRUCTION STONES AFFECTED BY HIGH TEMPERATURES

In the following subsections, the compressive strength, elastic modulus, peak strain, Poisson's ratio and tensile strength are presented in the same way as above, i. e. showing the data from all the considered references and then proposing the mean and 65-quantiles calculated on such bases. The details of the testing conditions for mechanical tests (sample shape and size, heating rate, duration at maximum temperature, cooling regime and load/displacement/stress rate) are listed in Table A6 in the Appendix. Figure 10 shows a typical testing machine for compression of small samples, with different setups for compressive test, measurement of strain for the calculation of elastic modulus and Poisson's ratio and indirect tensile (Brazilian) test. It should be noted that, due

to the lack of standards, the tests presented henceforth feature very different conditions in high temperature exposure and testing parameters. The effects of parameters other than the maximum temperatures – i. e. the heating rate, duration and cooling regime – may be very variable on the residual properties of porous construction materials, see subsection 5.3 below.
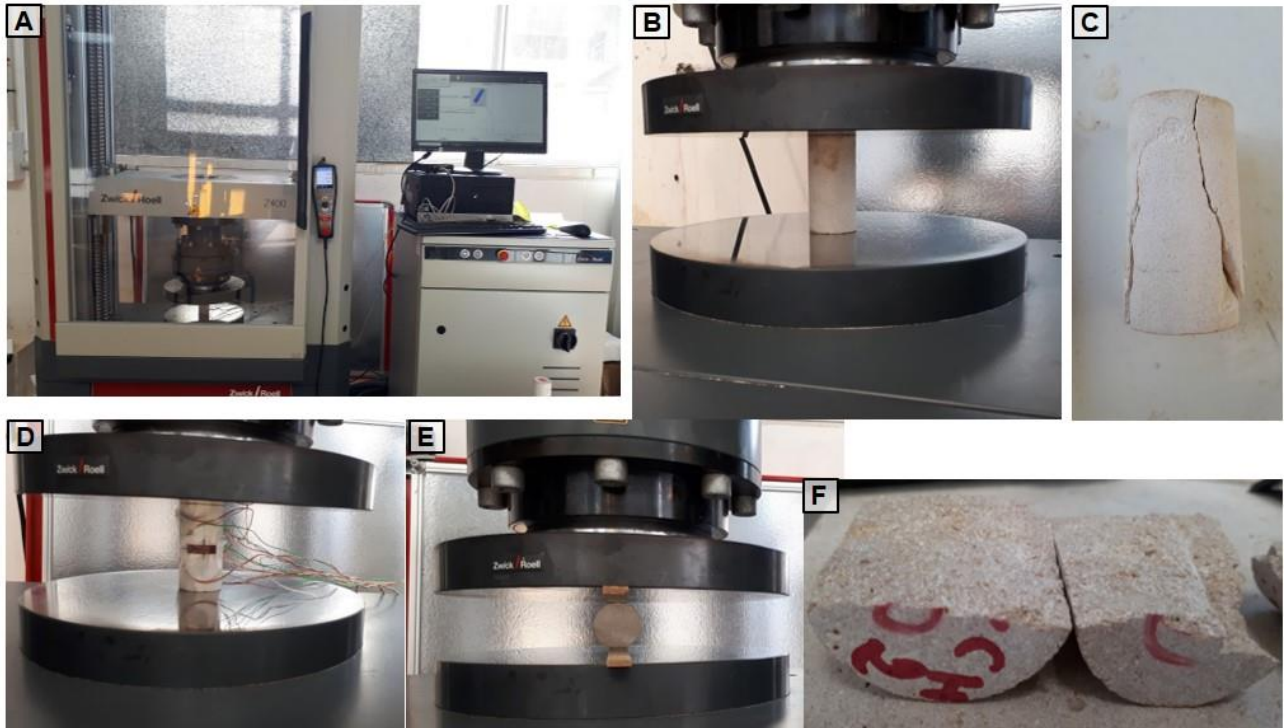


**Figure 10.** A) Equipment for mechanical tests: Zwick & Roell Z400 press and acquisition unit, B) sample under compression, C) compressive rupture, D) sample instrumented with gauges for the measurement of strain, E) indirect tensile test, and F) indirect tensile rupture [43]

## 4.1. Compressive strength $f_{c,T}$ as a function of temperature

Figure 11 presents the compressive strength $f_{c,T}$ as a function of temperature for granites (A), marbles (B), sandstones (C) and limestones (D), from the considered references.
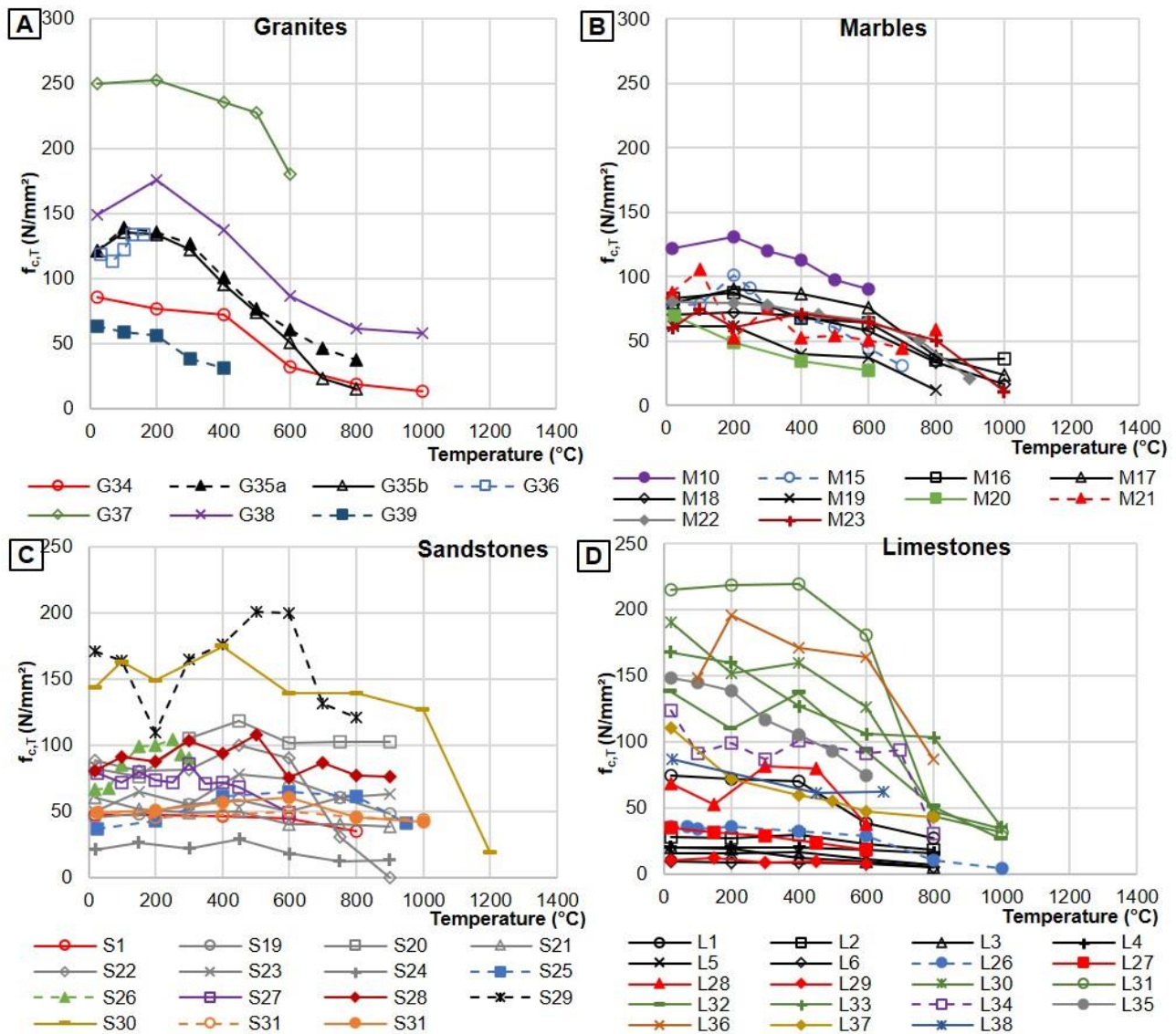
**Figure 11.** Residual (solid lines) and hot (hyphened lines) compressive strength of granites (A), marbles (B), sandstones (C) and limestones (D) after high temperatures [32, 35, 39, 43, 60, 61, 62-80].

The graphs of Figure 11 account for residual strength after high temperature exposure, and include also the few available tests under high temperatures ('hot' conditions, hyphened lines). All the latter tests were performed by loading the specimens after the target temperature was attained.

Generally, all the types of stone show very little or no strength decay until 200°C. Some slight increase is possible at 200°C, e. g. G35-36-38 (Figure 11A), M15 (Figure 11B) and L36 (Figure 11D), and at around 500°C for sandstones (Figure 11C). From 400°C on, the strength decrease is neat enough for granites, marbles and limestones, while sandstones appear to be less sensitive, from this point of view, to high temperatures. Two cases allow appreciating the performance of the same rock under and after exposure, i. e. the granite G35 [63] and the sandstone S31 [75]; the comparison reveals, in both cases, almost negligible differences in the values of hot and residual strength. This shows that, in such cases, any strength recover or damage development are negligible after cooling,

19

at least in the short term as per experimental procedures. Finally, Figure 11A-D enlighten the wide range of strength even within the same type of stone, namely 60-250 N/mm² for granites, 60-120 N/mm² for marbles (but values are mostly concentrated in an interval of 60-90 N/mm²), 20-170 N/mm² for sandstones and, the largest of all, 10-215 N/mm² for limestones. Just because of the wide scatter of the original values, it is significant to analyse the trends of the normalised residual strength $f_{c,T,res}/f_c$ for granites (Figure 12A), marbles (Figure 12B), sandstones (Figure 12C) and limestones (Figure 12D).
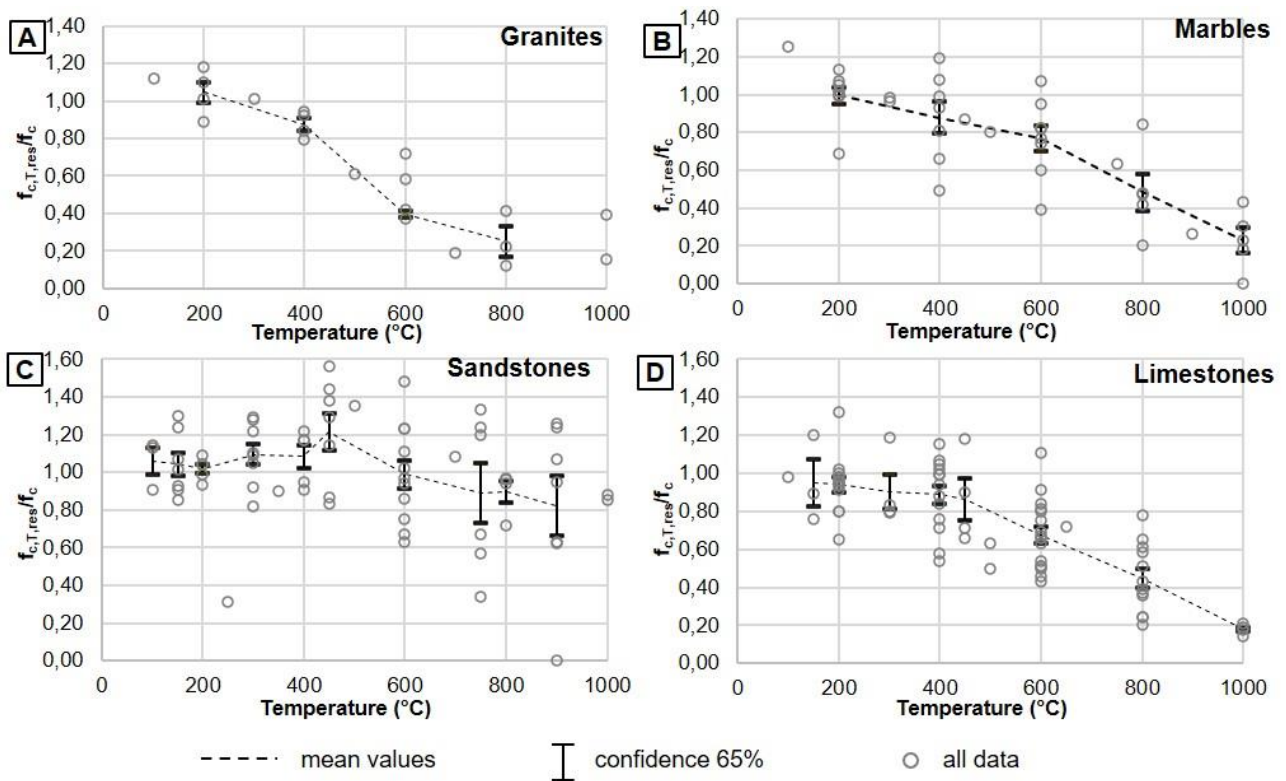


**Figure 12.** Mean values and 65-quantiles of normalised residual compressive strength for A) granites, B) sandstones, C) marbles and D) limestones

The graphs in Figure 12 confirm that the decrease in $f_{c,T,res}$ becomes significant from 400°C for granites (especially), marbles and limestones, and from 500°C for sandstones. The confidence intervals are narrow enough; data are fewer but very uniform for granites, while the widest intervals are for sandstones beyond 600°C and limestones at 100-300°C. All of them are fairly enough described up to 800°C.

Finally, Figure 13 shows the mean values and 65% interval of confidence for the few available data about normalised compressive strength under the action of high temperatures $f_{c,T,hot}/f_c$, which cover granites (Figure 13A) and sandstones (Figure 13B). In fact, the experimental data for marbles and limestones do not allow establishing significant mean values. For granites, only the 65% confidence interval at 100°C could be determined; the data could only suggest a decreasing trend. As for

sandstones, the mean values show negligible variations from 200°C to 800°C, but the dispersion is very high and cannot help establishing a reliable trend.
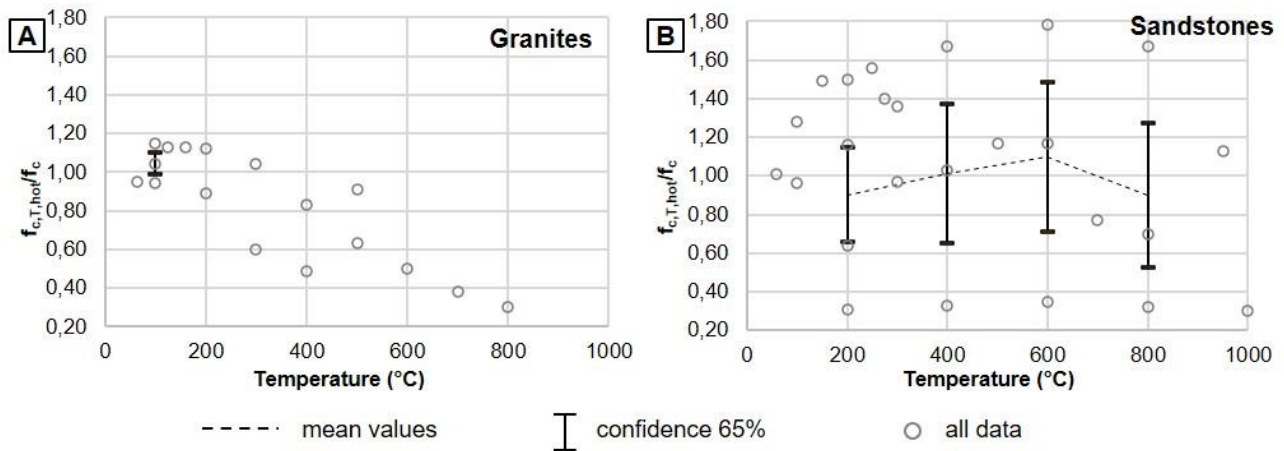


**Figure 13.** Mean values and 65-quantiles of normalised hot compressive strength for A) granites and B) sandstones

## 4.2. Static elastic modulus $E_T$ as a function of temperature

The static elastic modulus is generally calculated after strain measurements taken during compressive tests by means of vertical strain gauges. Samples can be similar to the ones used for compressive tests, but they must have at least a 2:1 height-to-width ratio; for instance, a standard protocol for normal temperature tests is EN 12407 [81]. Additionally, if horizontal strain gauges can be attached to the sample, the Poisson's ratio can also be calculated.

Data for the elastic modulus of stones as a function of temperature are shown in Figure 14, which displays the $E_T$-$T$ graphs for granites (Figure 14A), marbles (Figure 14B), sandstones (Figure 14C) and limestones (Figure 14D).

The data for $E_T$-$T$ are fewer than for compressive strength, and the scatter of original values is as high, i. e. 15000-40000 N/mm² for granites, 18000-54000 N/mm² for marbles, 10000-50000 N/mm² for sandstones and, the largest of all, 10000-72000 N/mm² for limestones. At increasing temperatures, the decreasing trend prevails; the higher is the original stiffness, the faster appears the decline, e. g. G38, M20, L35. In some cases, i. e. granites G34-35-36, marbles M21-22, and limestone L34 the decrease in $E_T$ begins at 300°C; for sandstones, the initial unchanged branch can extend even up to 400-600°C (S26-28-29-31) and include negative or positive peaks, or both (S30-31). Beyond 600°C, in all cases, the reduction in material's stiffness is mostly dramatic.

The lines connecting the mean values and the 65% confidence intervals for the normalised residual elastic modulus $E_{T,res}/E$ as a function of temperature $T$ are illustrated in Figure 15A for granites, Figure 15B for marbles, Figure 15C for sandstones and Figure 15D for limestones. The mean lines confirm the monotonically declining trends for granites, marbles and limestones, while the average behaviour of sandstones can be deemed constant up to 400°C, followed by a neat decrease at

600°C and recover at 800°C. However, the confidence is loose for marbles, sandstones and, up to 400°C, for granites; quite the opposite, limestones show good enough confidence up to 800°C.



**Figure 14.** Residual (solid lines) and hot (hyphened lines) elastic modulus of granites (A), marbles (B), sandstones (C) and limestones (D) after high temperatures [39, 60-63, 66-75, 77-79, 82-84]

Finally, the collected data about $E_T$ under high temperatures (hyphened lines in Figure 14) allow for plotting the graphs of mean values and 65-quantiles for the hot normalised modulus $E_{T,hot}/E$ of granites (Figure 16A) and sandstones (Figure 16B). Alike the hot compressive strength, only the 65-quantile at 100°C could be determined for granites, and the whole set of data can only partially suggest a decreasing trend. For sandstones, the confidence is appreciably better for hot (Figure 16B) than for residual values (Figure 15C); changes are negligible up to 600°C, then at 800°C the $E_T/E$ value is only slightly higher than the residual one at the same temperature (Figure 15B). Comparing Figures 15C and 16B, especially at 600°C, it is interesting to notice that the residual $E_T$ of sandstones is largely affected by the residual micro-cracking from the α- to β-quartz inversion and

the possible damage in the cooling phase; in this case, the material's performance can be deemed worse after than under heating.



**Figure 15.** Mean values and 65-quantiles of normalised residual elastic modulus for A) granites, B) sandstones, C) marbles and D) limestones



**Figure 16.** Mean values and 65-quantiles of normalised hot elastic modulus for sandstones

### 4.3. Peak compressive strain $\varepsilon_{c1,T}$ as a function of temperature

At the original state, values of $\varepsilon_{c1}$ are uniform enough for granites and sandstones in the range 0.3-1.7% (Figures 17A and 17C), and for marbles and limestones in the range 0.2-0.8% (Figures 17B and 17D). As the graphs in Figure 17A to 17C demonstrate, $\varepsilon_{c1,T}$ generally increases at increasing

temperature. The increase becomes higher after 400°C-600°C, and in some cases the effect of the α- to β-quartz inversion is an evident increase in peak strain, e. g. G35, G37, S27 and S28.
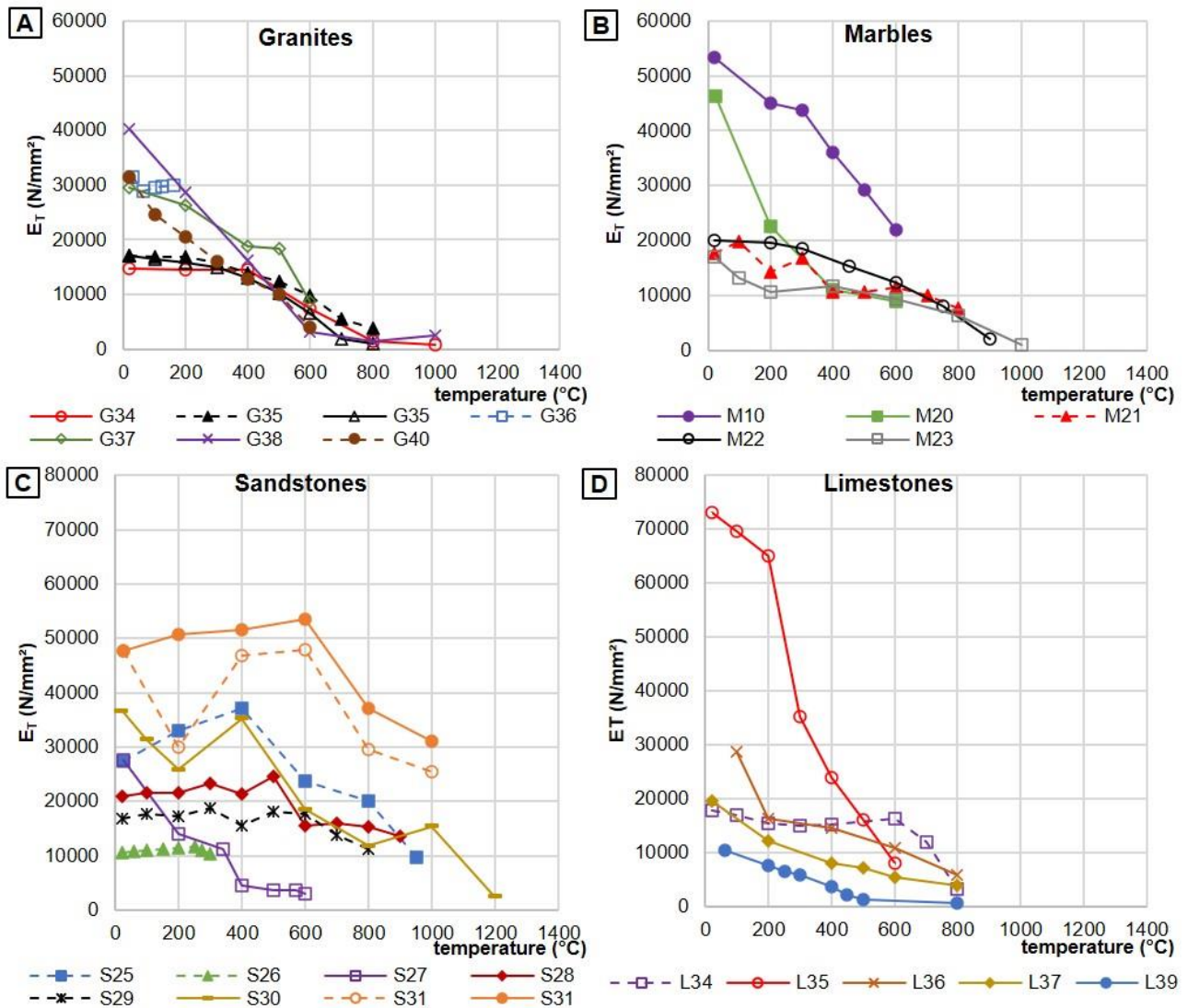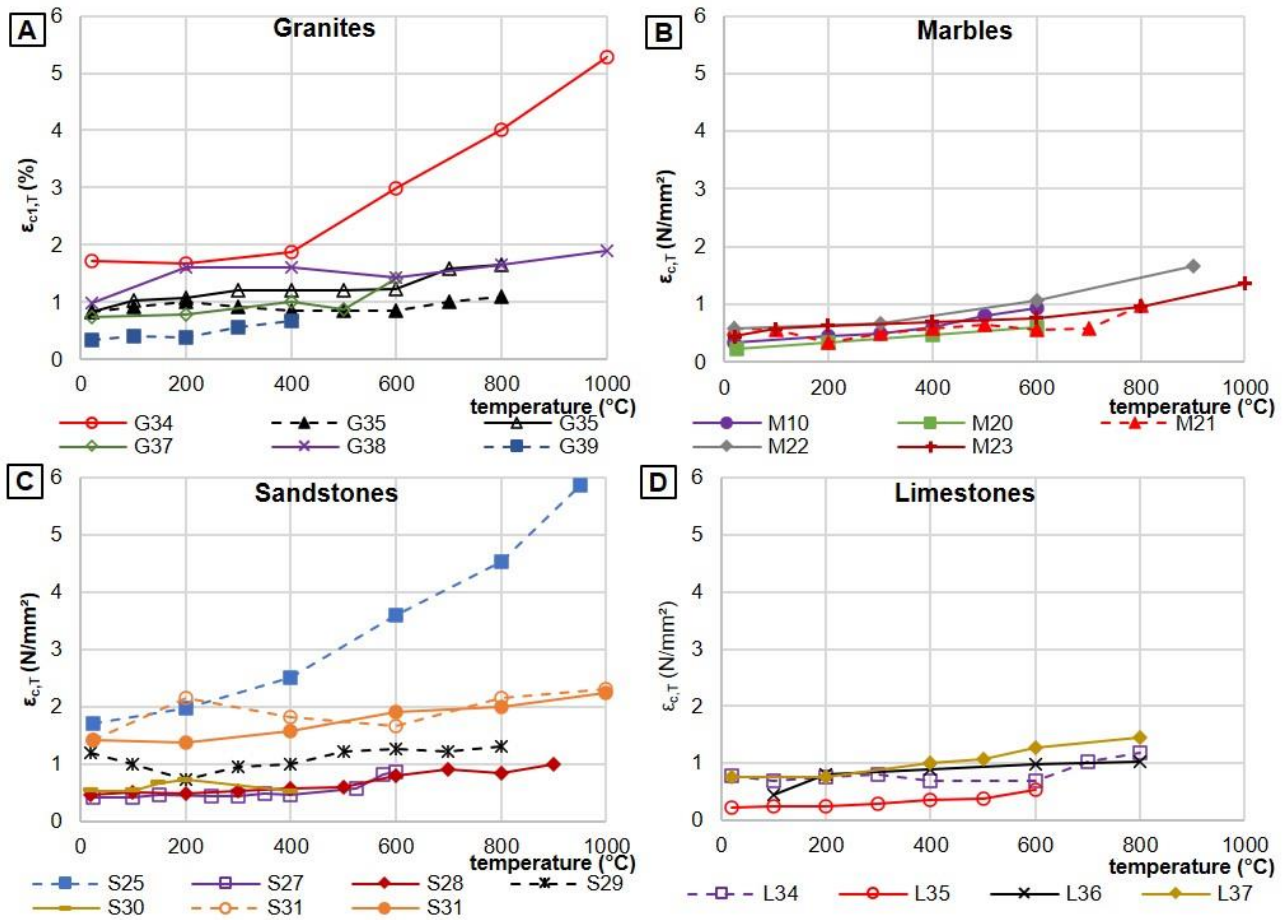


**Figure 17.** Residual (solid lines) and hot (hyphened lines) peak compressive strain of granites (A), marbles (B), sandstones (C) and limestones (D) after high temperatures [39, 60-63, 66-70, 72-75, 77-79, 85]

The increasing trends are generally confirmed by the graphs of the mean values and 65% confidence intervals of the residual normalised peak compressive strain $\varepsilon_{c1,res,T}/\varepsilon_{c1}$ for granites (Figure 18A), marbles (Figure 18B) and limestones (Figure 18D); a constant behaviour followed by increase from 400°C on is established for sandstones (Figure 18C). The amount of data on which the graphs are based is not large, but at least for granites from 200 to 800°C, and especially sandstones from 100 to 600°C, it allows for a pretty good level of confidence. For marbles and limestones, a steeply increasing trend is described from 200 to 600°C, but with not negligible dispersion.

The means and 65% confidence intervals for the normalised peak compressive strain in hot conditions $\varepsilon_{c1,hot,T}/\varepsilon_{c1}$ can give only information for sandstones (Figure 19). The latter shows, beyond 400°C, a less distinct increase than the residual values (Figure 18C), i. e. at 600°C $\varepsilon_{c1,hot,T}/\varepsilon_{c1}$ is about 1.40, while $\varepsilon_{c1,res,T}/\varepsilon_{c1}$ is about 1.80; this can confirm the effect of micro-cracking as in the comparison of $E_{T,res}$ to $E_{T,hot}$.
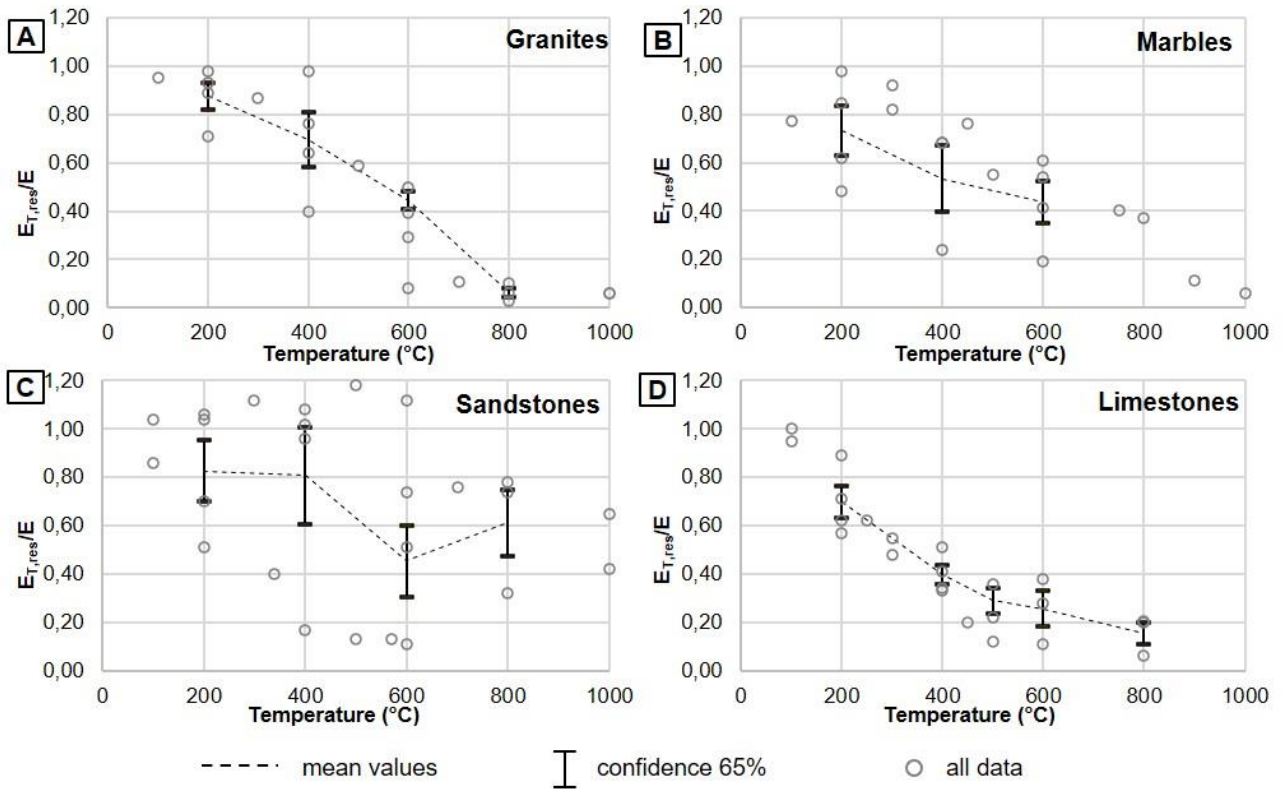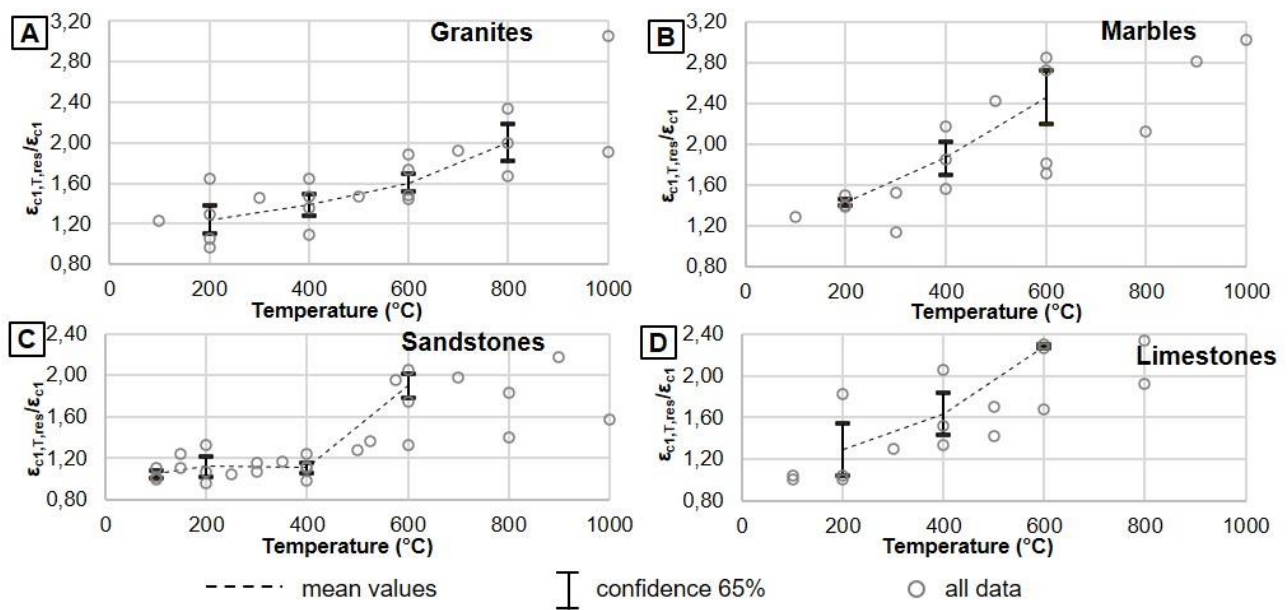
**Figure 18.** Mean values and 65-quantiles of normalised residual peak compressive strain for A) granites, B) sandstones, C) marbles and D) limestones
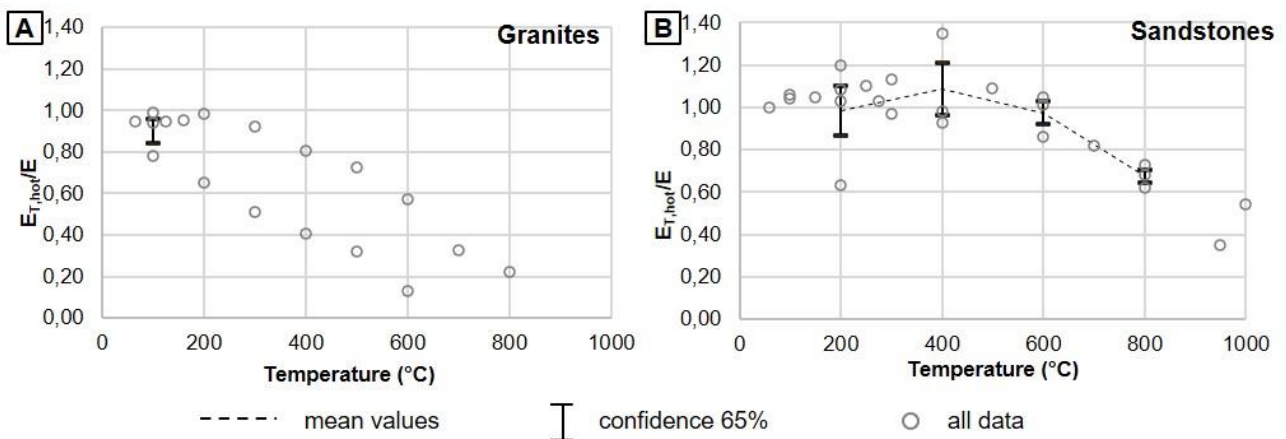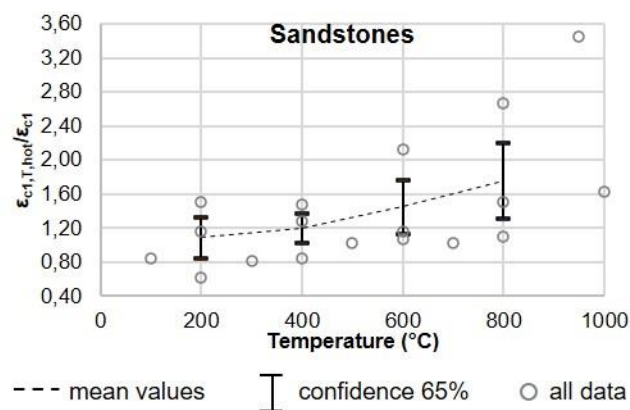


**Figure 19.** Mean values and 65-quantiles of normalised hot peak compressive strain for sandstones

### 4.4. Poisson's ratio $v_T$ as a function of temperature

Very scarce experimental information is available about the temperature-dependent Poisson's ratio of granites (Figure 20A), marbles (Figure 20B), sandstones (Figure 20C) and limestones (Figure 20D). The original values lie between 0.18-0.28 for all the types of stone. Similarities can be recognised between granites and sandstones; in such cases, the residual Poisson's ratio $v_T$ decreases very slightly (until 300-500°C) and then starts increasing up to higher values than the original at 800-1000°C. The only two data series describing the temperature-dependence of $v_T$ for marbles and limestones also appear similar to each other, in showing the most significant decrease at 200°C; then, the marble shows negligible variations up to 600°C, while the limestone gradually decreases. Two data series relate to $v_T$ measured in 'hot' conditions, concerning granites G36 and G37; such data suggest that, during heating, Poisson's ratio increases, taking a steeper rise after

400°C. Finally, G35 and S31 allow for comparing slow (b) and fast (c) cooling effects, showing no relevant variations.
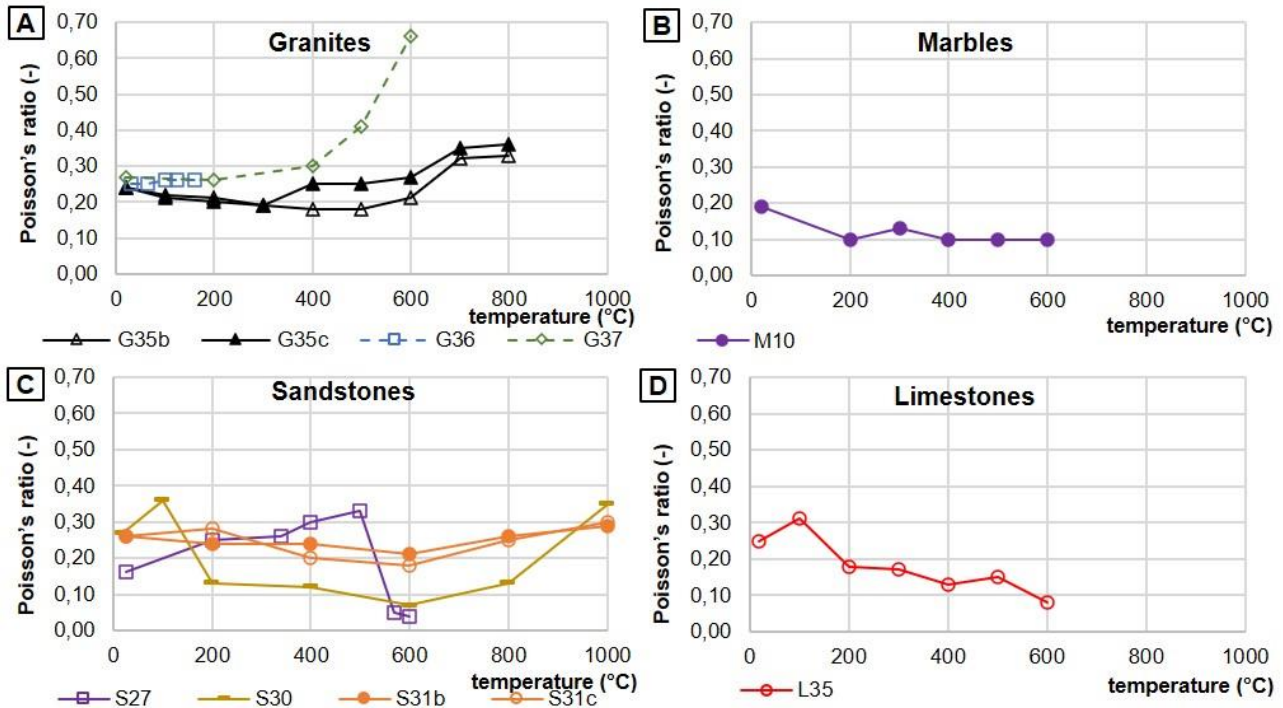


**Figure 20.** Residual (solid lines) and hot (dotted lines) Poisson's ratio of granites (A), marbles (B), sandstones (C) and limestones (D) after high temperatures [39, 60, 61, 67, 74, 75, 77]

The mean and 65-quantiles could be calculated only for the normalised residual Poisson's ratio $v_{T,res}/v_T$ of sandstones (Figure 21). The values describe an appreciable decrease in $v_T$ from 400°C to 600°C, with very wide intervals of confidence from 200 to 400°C.
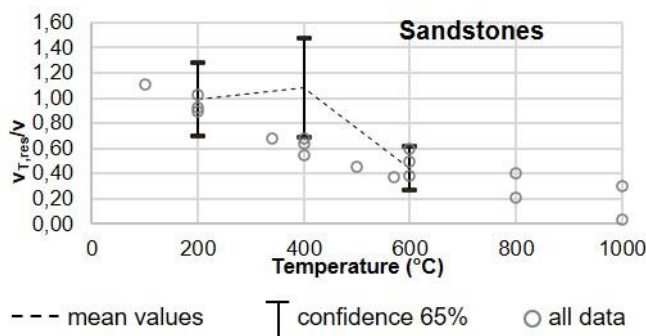


**Figure 21.** Mean values and 65-quantiles of normalised residual Poisson's ratio for sandstones

4.5.    Tensile strength $f_{t,T}$ as a function of temperature

In problems of structural engineering, masonry is often considered, on the safe side within simplified approaches, a no-tension material. However, structural analyses aimed at a higher degree of accuracy require the input of materials' tensile strength to describe the nonlinear behaviour of masonry in compression and shear. Experimental information about the tensile strength of stones is

reported in Figure 22A for granites, Figure 22B for marbles, Figure 22C for sandstones and Figure 22D for limestones. Data are abundant as far as they concern the residual $f_{t,T}$ of limestones, and a good enough amount of data series is available for marbles; quite the opposite, experimental information is insufficient for granites and sandstones. As well, experimental information does not adequately cover the tensile behaviour of rocks during exposure to high temperatures.
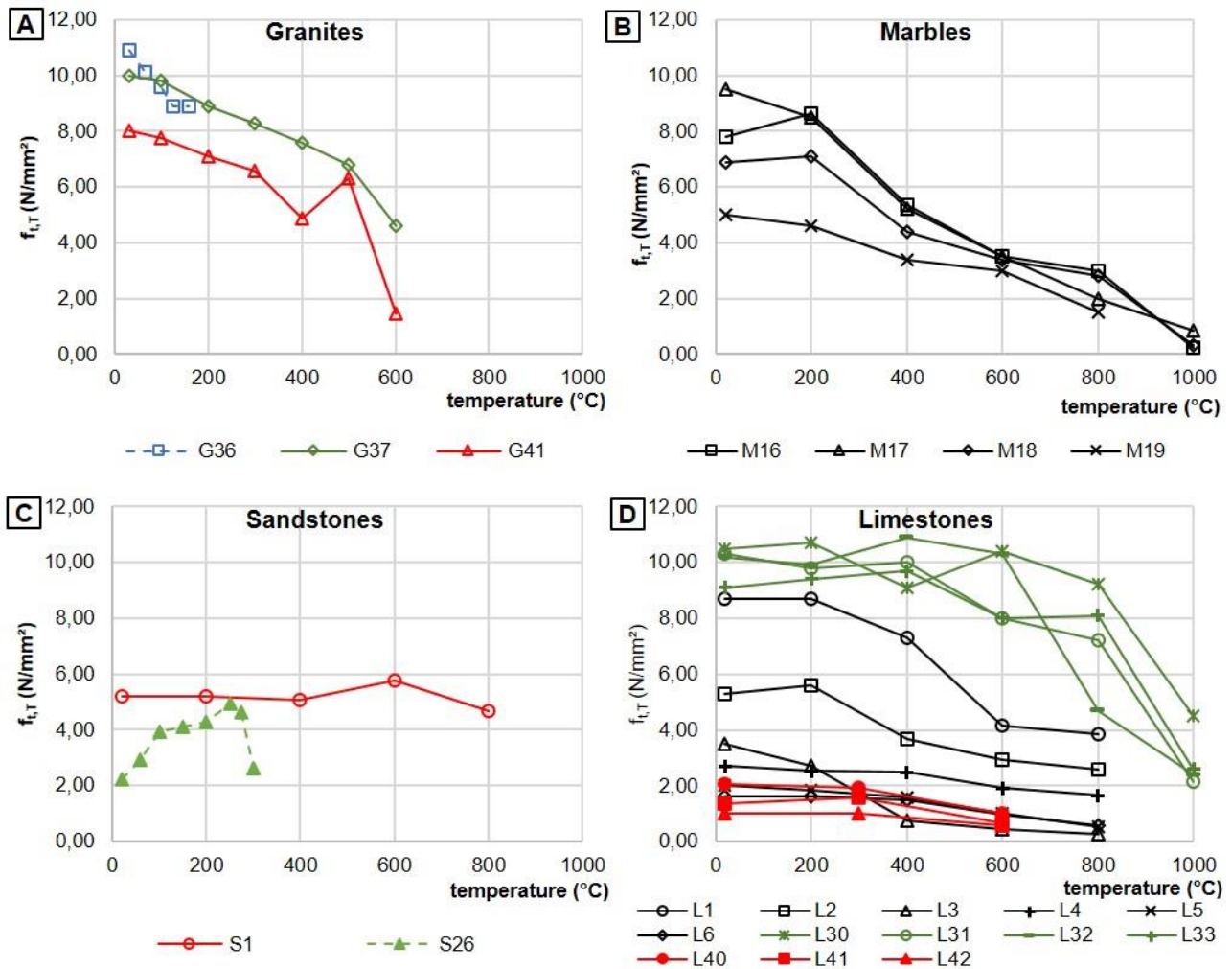


**Figure 22.** Residual (solid lines) and hot (dotted lines) tensile strength of granites (A), marbles (B), sandstones (C) and limestones (D) after high temperatures [35, 39, 43, 60, 71, 86]

Like noticed about the compressive strength, the original values of tensile strength $f_t$ span across a wide range, namely 1-10 N/mm² for limestones and 5-10 N/mm² for marbles. The two data series for sandstones appear discordant, while granites are at least in a good enough agreement. The $f_{t,T}/T$ trend is declining in all cases illustrated in Figure 22. For limestones and marbles, the features of residual behaviour look quite clear; the tensile strength decay mostly develops between 200 and 600°C, followed by a more stable phase and finally a steeper loss from 800°C on. The few data about granites indicate that the quartz inversion between 500 and 600°C may result in a faster loss of compressive strength (G41).

Finally, the normalised residual tensile strength, calculated for marbles (Figure 23A) and limestones (Figure 23B) shows quite good levels of confidence over a wide temperature range (200 to 1000°C). Marbles present a monotonically decreasing behaviour, reaching almost zero strength after exposure to 1000°C; limestones undergo monotonic decay from 300°C on, retaining about the 30% of original strength after exposure to 1000°C.
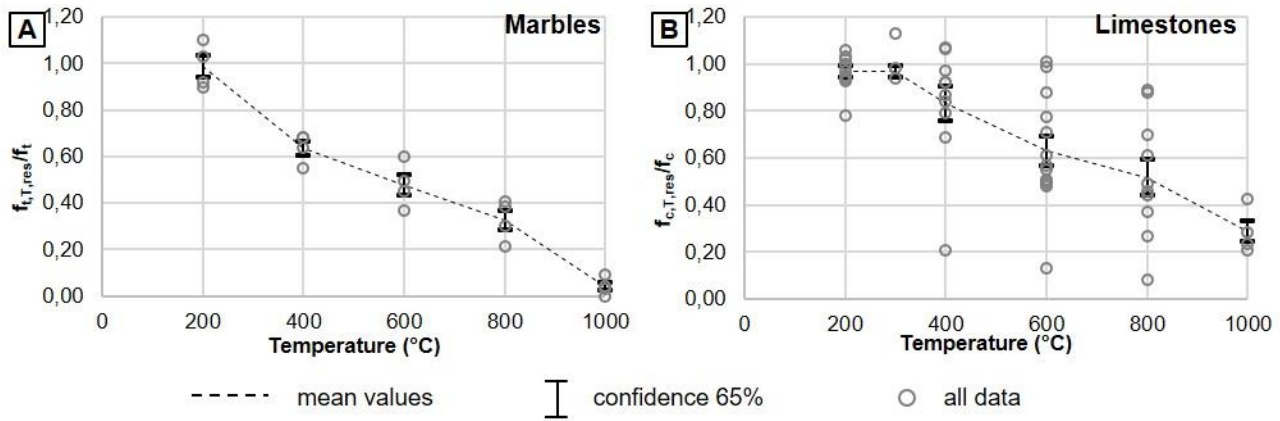


**Figure 23.** Mean values and 65-quantile of normalised residual tensile strength for A) marbles and B) limestones

# 5. EFFECTS OF DIFFERENT PARAMETERS ON THE THERMAL AND MECHANICAL PROPERTIES OF CONSTRUCTION STONES

The following subsections report the available information of the influence of porosity, water content, anisotropy and characteristics of thermal stress history on the above described thermal and mechanical properties.

## 5.1. Effect of porosity and moisture level

The beneficial effect of porosity in accommodating thermal strain under high temperatures has already been mentioned in subsection 2.3.

At normal temperatures, the thermal conductivity $\lambda$ is related to the porosity $\phi$ of a rock, as a result of the lesser heat conduction in air than in the solid phase. Total porosity generally increases at increasing temperatures, depending on the development of micro-cracking and the thermal dilatation of constituent minerals [28]. According to different studies, porosity – as well as the mean pore size, and the number of larger pores – increases in a relevant way from 400°C on; such temperature also marks a significant decrease in the conductivity of sandstone [56] and in the compressive strength of limestone, as well [35]. In fact, rocks with low initial porosity are particularly prone to micro-cracking under high temperatures. This can be due to the build-up vapour pressure inside the pore network, which finally reduces the compressive strength; vice versa, highly porous rocks provide escape paths

28

for vapour, resulting in lesser sensitivity to the effects of pore pressure [80]. On the other hand, crack propagation is easier in compact media than in porous ones, without the pores stopping and slowing down the propagation of cracks. Very compact rocks, like granite and marble, have fragile mechanical behaviour and the vapor pressure effect can become less important, especially with a slow heating rate. Parabolic (for sandstone, [56]) and exponential (for marble, [65]) porosity-temperature relationships were empirically established. Such relationships can be a useful tool for estimating *a posteriori* the maximum temperature experienced by a stone masonry structure during a fire, if the porosity of a fire-exposed sample can be measured [65].

Research on the water absorption of construction stones provides abundant information [87]. A higher water absorption brings on a higher increase in conductivity, as compared to the dry state, but only until a certain level of porosity [51, 88]. Čermák and Rybach [50] proposed an exponential relationship between $\lambda$ and $\phi$ for sedimentary rocks, holding until porosity values of 0.2-0.3, considering $\lambda_d$ and $\lambda_w$ respectively as the conductivity of the dry and wet rock, (Equation 7)

$$\lambda_w = \lambda_d \cdot \exp(0.024\phi) \tag{7}$$

The effect of the moisture level is remarkable in rocks with high content in quartz (Figure 24A), while water saturation only slightly increases the conductivity of calcareous stones (Figure 24B).
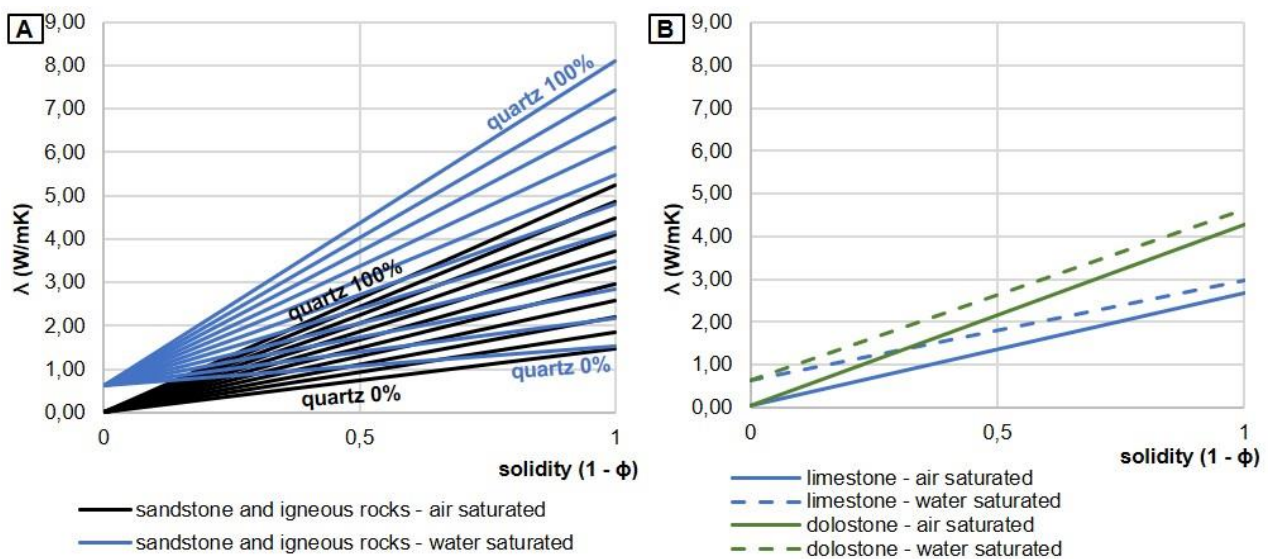


**Figure 24.** Thermal conductivity at varying solidity of A) quartz-rich rocks (igneous and sandstones) and B) dry and water-saturated calcareous stones

A linear expression (Equation 8 [51, 89]) can apply to sedimentary rocks up to 500°C exposure; beyond such value, the effect of radiative heat flux in the pores becomes not negligible [89].

$$\lambda_w = \lambda_d \cdot (1 - \phi) \tag{8}$$

In heat conduction problems, Robertson [51] suggests adopting the bulk density in order to account for porosity in the value of specific heat at constant pressure $c_p$; either, the specific heat, measured or calculated with Equation 6, can be multiplied by the rock solidity $(1 - \phi)$.

Concerning the effect of moisture on the mechanical properties of rocks, studies on different types of sandstones agree about the moisture-dependent decrease in strength at ambient temperature. Such decay can due to decrease in capillary tension, increase in pore pressure, reduction of the fracture surface energy, reduction of internal friction and chemical deterioration, possibly acting at the same time [90]. The mechanical decay of sandstone in saturated condition is significant, e. g. a -25% in compressive strength and elastic modulus [91]; however, it can be much more dramatic, e. g. -40 to -60% in compressive strength for ferruginous sandstone [92], or even -90% in compressive strength, -93% in elastic modulus and -90% in tensile strength for fine-grained sedimentary rocks [93]. Small variations in density (1700–2300 kg/mm$^3$) can lead to large variations in strength (1–25 N/mm$^2$); as well, saturated samples show earlier crack initiation and a less brittle failure mode, which indicates the deterioration of the frictional resistance [92]. Other studies have reported that the peak compressive strain does not depend on moisture [94].

*5.2. Effect of anisotropy*

As noted in Section 2 (Table 1), anisotropy especially affects the properties of metamorphic rocks. This characteristic is one of the main sources of thermally induced mechanical damage that could affect stones. Within the same type of rock, there can be isotropic or anisotropic species, taking as reference the bedding plane; depending on the maximum attained temperature, isotropic or anisotropic rocks can exhibit residual thermal strain or none [49]. In anisotropic stones, the axis of maximum residual strain is not necessarily the same of maximum strain under target temperature [87]. Table 4 lists values of maximum and residual strain for some anisotropic rocks.

**Table 4.** Maximum and residual strain of anisotropic rocks after heating at target temperatures

| Stone type | Porosity (%) | Temperature (°C) | Maximum strain (%) | Residual strain (%) |
|---|---|---|---|---|
| Granite, India [44] | - | 1000 | 2.45(X); 2.30(Y); 2.23(Z) | 1.30(X); 1.15(Y); 1.13(Z) |
| Granite, Sardinia [44] | - | 1000 | 2.46(X); 2.27(Y); 2.29(Z) | 1.52(X); 1.44(Y); 1.32(Z) |
| Granite, Czech Republic [44] | - | 1000 | 2.95(X); 2.85(Y); 2.64(Z) | 1.97(X); 1.83(Y); 1.76(Z) |
| Limestone, Germany [26] | 4.64 | 950 | 2.83 ($\perp$ bedding) | 0.69 ($\perp$ bedding) |
| | | | 2.45 (// bedding) | -0.68 (// bedding) |
| Glauconitic sandstone, CZ [46] | - | 950 | 1.88(X); 1.95(Y); 1.89(Z) | 0.87(X); 0.92(Y); 0.88(Z) |
| White sandstone, [46] | - | 950 | 1.80(X); 1.84(Y); 1.88(Z) | 0.28(X); 0.29(Y); 0.33(Z) |
| Reka sandstone [46] | - | 950 | 1.91(X); 2.00(Y); 1.95(Z) | 0.96(X); 0.97(Y); 0.92(Z) |
| Doubrava sandstone [46] | - | 950 | 1.95(X); 1.90(Y); 1.94(Z) | 0.73(X); 0.70(Y); 0.77(Z) |
| Gypsum [26] | 1.10 | 950 | 1.30 ($\perp$ bedding) | -2.10 ($\perp$ bedding) |
| | | | 0.70 (// bedding) | -3.50 (// bedding) |

Calcite-bearing stones usually show anisotropic thermal expansion, which results in dilatation perpendicular to the bedding plane and contraction parallel to it. Finally, the thermal strain of gypsum is highly anisotropic and exhibits a dilatation followed by a contraction up to about 300°C, due to

dehydration. After a reprise of thermal dilatation, shrinking occurs after 800°C, leaving a remarkable negative residual strain, higher in direction parallel to bedding [26]. Information is available about the anisotropy factor of thermal conductivity – i. e. the ratio of the property parallel to bedding to the same property perpendicular to bedding, $\lambda_{//}/\lambda_{\perp}$ – for marbles (1.02-1.06), granites (1.30-1.40), limestones (0.93-1.35) and sandstones (1.04-1.19), [50, 51]. Some examples [25, 50] are illustrated in the graph of Figure 25.
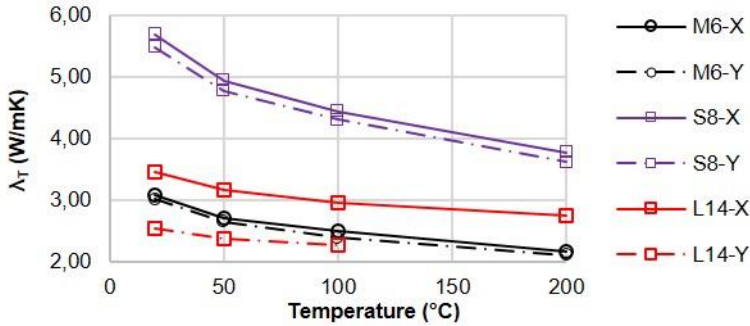


**Figure 25.** Anisotropic conductivity of marble M6, sandstone S8 and limestone L14 [25, 50]

According to experimental evidence on igneous rocks – but this also holds for quartz and calcite rocks – the anisotropy of thermal conductivity is strongly reduced at high temperatures [52, 95]. Finally, water saturation does not significantly affect a rock's thermal anisotropy [95].

*5.3.    Effects of multiple thermal stress, heating-cooling cycles and cooling regime*

Literature provides some information about the effect of subsequent thermal stresses on the thermal strain of marble M1 and sandstones S3 and S4, all taken from [25] (Figure 26). The thermal strain capacity of all the three materials is remarkably reduced after the first cycles and subsequent cooling. In fact, at 600°C, M1 shows a -33% strain from first to second cycle. At 1000°C, S3 shows a reduction of -63% and -77% for the two different types of second thermal stress, i. e. second cycle and use in a glass furnace (which heats up to 1400°C). Finally, at 594°C S4 shows a -59% in thermal strain from first to second cycle. The results of S3 and S4 indicate that the effect of quartz transition can still be noticed in the second heating; S3 also shows very little differences between a second cycle at 1000°C maximum temperature, and the use in a glass furnace (reaching 1400°C).
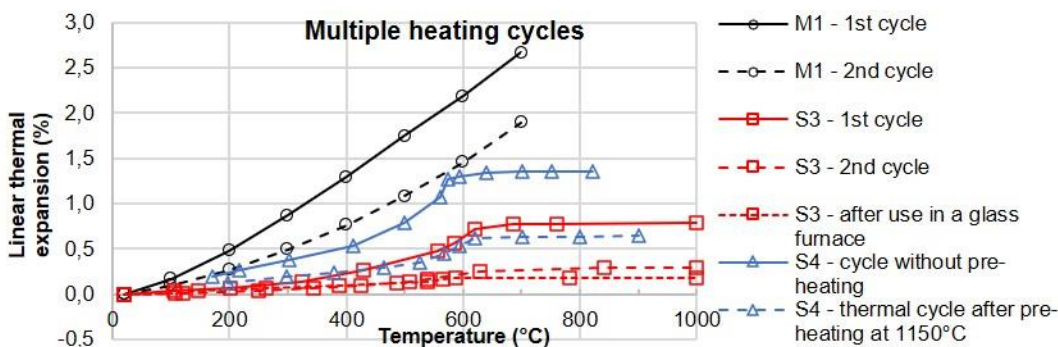


**Figure 26.** Thermal strain of marble M1 and sandstones S3 and S4 for different heating cycles

The residual thermal conductivity, at least shortly after cooling as it happens in laboratory procedures, is far lower than the original value, especially because of increased porosity. As demonstrated by the cases illustrated in Figure 27, the decrease in $\lambda_T$ does not stop at the maximum reached temperature; the parameter is significantly lower at the beginning of the cooling phase (after constant maximum temperature) than at the end of heating, and can very partially recover only at the very end of cooling.
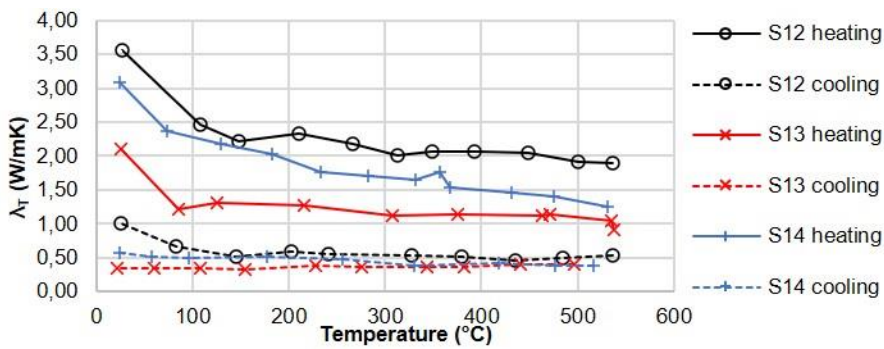


**Figure 27.** Thermal conductivity during heating-cooling cycles for sandstones S12, S13 and S14

As far as the mechanical properties are concerned, some information is useful to enlighten the effects of hot condition and different cooling regimes on the compressive strength, elastic modulus and peak compressive strain of a granite and a sandstone [63, 75]. The data series of G35 and S31 already presented in Section 4 are collected here in Figure 28 to emphasise the mutual comparison of $f_{c,T}$ (Figure 28A), $E_T$ (Figure 28B) and $\varepsilon_{c1,T}$ (Figure 28C) at hot state, slow cooling in air and fast cooling (water quenching). The two types of stone behave very differently as far as it concerns the strength and stiffness, but someway similarly regarding the peak compressive strain. In detail, the compressive strength (Figure 28A) of the granite undergoes an initial increase followed by decrease, while the sandstone – as already noted in Section 3 – is much less sensitive to the high temperature treatment. The former shows no relevant differences between the hot condition and slow cooling, while the latter displays some performance improvement after slow cooling. In both cases, the fast cooling negatively affects the residual strength, especially for granite. The elastic modulus (Figure 28B) of the granite decreases at increasing temperatures without large differences among the three conditions, being the hot condition the least damaged. Quite differently, the slow cooling appreciably mitigates the effects of thermal damage for the sandstone, while the water quenching is just as damaging as the hot condition. Finally, the peak compressive strain (Figure 28C) shows some similarities between the granite and the sandstone. In fact, the subsequent phases of increase up to 200°C, decrease up to 600°C and then increase, at the hot state, are visible for both rocks and much more evident for the sandstone. The slow cooling brings on a neat increase in the peak strain for the granite, and a progressive increase from 200°C on for the sandstone. The fast cooling entails, for the granite, peak strain decrease until 200°C and then increase up to the highest values; for the sandstone, the behaviour after water quenching repeats that at hot conditions, but with larger

32

decrease in the peak strain between 400 and 600°C. This leads to confirm that the extinction of a fire with water could bring on deleterious consequences on the material's stress-strain behaviour of stone masonry units.
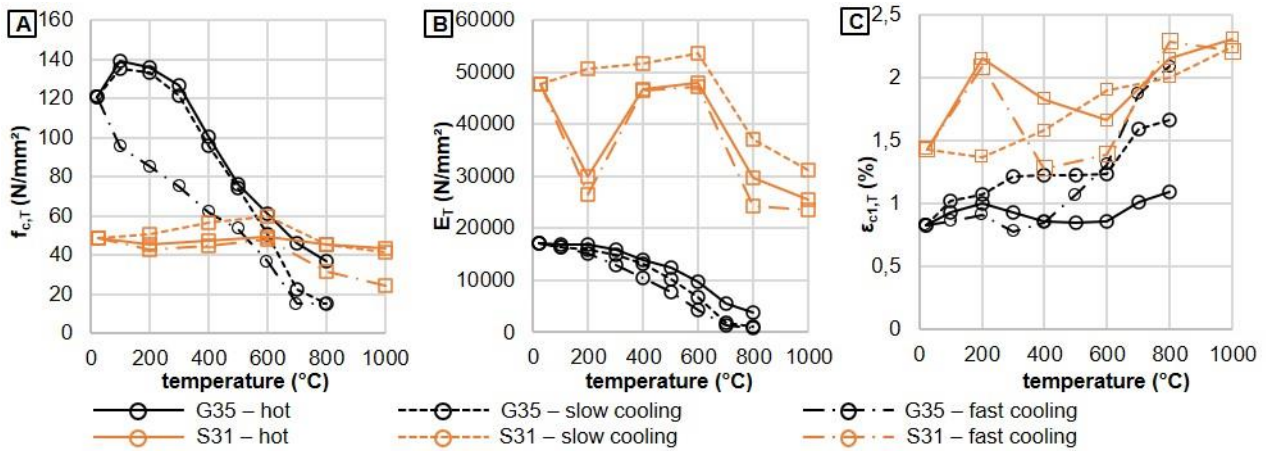


**Figure 28.** Effects of hot condition, slow cooling and quenching on the compressive strength (A), elastic modulus (B) and peak compressive strain (C) of granite G35 and sandstone S31

6. CONCLUSIONS

The following conclusions summarise the information reported in the paper – derived from about 80 references – for each type of stone, to enlighten the peculiar characteristics for implementation in analytical performance-based design calculations, as well as the detailed research needs.

- The behaviour of granites and sandstones under and after exposure to high temperatures is mainly affected by the processes of dehydroxilation of phyllosilicates and clay minerals (possible from 200°C on), and α- to β-quartz expansive inversion (at 573°C). For marbles and limestones, the chief influence is that of decarbonisation (from 650 to 950°C) and portlandite formation (in the cooling phase).

- The trends of thermal expansion of granites, marbles, sandstones and limestones are quite distinctive and enlightened by a good amount of data in a substantially good agreement. The temperature-dependent thermal expansion coefficient $\alpha_T$ increases at increasing temperature; it shows one or two peaks between 575 and 700°C due to quartz transformation in granites and sandstones, and reversal to negative beyond 800-900°C due to decarbonisation in limestones. The peak and reversal phases need more investigation to possibly reduce the scatter of data, as well as the thermal strain behaviour of marbles beyond 700°C.

- Concerning the temperature-dependent thermal properties $\lambda_T$ and $c_{p,T}$, the general trends – decreasing for $\lambda_T$ and increasing for $c_{p,T}$ at increasing temperature $T$ – are clear enough for granites, sandstones and limestones. The possibility of analytical evaluation of $\lambda_T$ and $c_{p,T}$ on the grounds of the component minerals is also a useful resource for scholars and designers. Research is particularly necessary for marbles, of which no useful mean values and 65-quantiles

could be determined. More insight is needed also for the specific heat of sandstones beyond 400°C, and of limestones between 300 and 500°C.

- The residual compressive strength as a function of temperature $f_{c,res,T}$ is well documented for all the considered construction stone types. The trends of the normalised residual strength are decreasing at increasing temperature for granites, marbles and limestones with substantially good confidence. The decrease becomes significant from 400°C on for granites, marbles and limestones, and from 500°C on for sandstones; the latter demonstrate a neatly lesser sensitivity to high temperatures from the point of view of compressive strength. For all the stone types, data provide a complete enough description of the $f_{c,res,T}/T$ behaviour up to 800-1000°C.

- The residual elastic modulus as a function of temperature $E_{res,T}$ shows a prevailing decreasing trend in all the considered stone types, with a possible initial unchanged phase; the average behaviour enlightens that $E_{res,T}$ remains constant up to 400°C in sandstones. In all cases, the stiffness reduction is dramatic beyond 600°C. However, data are significantly scattered for marbles, sandstones and, up to 400°C, for granites; this indeed enlightens a substantial research need. Only limestones show narrow enough 65% confidence intervals up to 800°C.

- The residual peak compressive strain $\varepsilon_{c1,res,T}$ generally increases at increasing temperature in granites, marbles and limestones, while sandstones rather show a constant phase up to 400°C followed by increase. The overall amount of data allows establishing the behaviour of granites up to 800°C and of sandstones up to 600°C with a pretty good level of confidence; on the other hand, more experimental data are needed to consolidate the knowledge of peak compressive strain of marbles and limestones after high temperature exposure.

- As for the Poisson's ratio, information is very scarce and can provide no useful quantitative figure.

- The collected data about the residual tensile strength $f_{t,res,T}$ allow to identify reliable declining trends in the 200-1000°C range for marbles and limestones; particularly for the latter, data are abundant. Quite the opposite, very scarce information is available about $f_{t,res,T}$ of granites and sandstones; indeed, research must be done on this topic.

- The available information about the compressive mechanical parameters in hot conditions ($f_{c,hot,T}$, $E_{hot,T}$, $\varepsilon_{c1,hot,T}$) is not abundant. On the grounds of the collected data, limited conclusions can only be made for sandstones. First of all, the available information shows negligible differences between the hot ($f_{c,hot,T}$) and residual strength ($f_{c,res,T}$), enlightening no significant recover after cooling. Sandstones retain more stiffness in hot than in residual conditions after exposure to >573°C, demonstrating the influence of micro-cracking due to the quartz inversion. This effect is confirmed also by the lesser increase in sandstones' peak strain in hot than in residual conditions. Finally, the tensile strength in hot conditions is another topic in need of investigation.

- The effects of porosity and water saturation are particularly relevant for the thermal and mechanical properties of quartz-rich stones. Formulations are available to take the effect of porosity into account while evaluating a rock's thermal properties.

- The influence of anisotropy should better be taken into account in the strain behaviour of metamorphic rocks, especially calcite- and gypsum-rich. However, more research is needed to clarify the extent of anisotropy at high temperatures.

- According to information about marbles and sandstones, the thermally-induced decay is generally irreversible after the first exposure to high temperatures. The cooling regime is also relevant; the available data demonstrate the negative effect of fast water cooling on the residual mechanical performance of granites and sandstones. This is a very important topic to be studied in view of the applications to historic stone masonry buildings attacked by fire.

REFERENCES

[1] M. Gomez-Heras, R. Fort (2009). Impacts of fire on stone-built heritage – An overview. J. Arch. Conserv. 15(2):47-58. DOI: 10.1080/13556207.2009.10785047

[2] F. Sciarretta (2014). Modeling of mechanical damage in traditional brickwork walls after fire exposure. Adv. Mat. Res. 919-921:495-499. DOI: 10.4028/www.scientific.net/AMR.919-921.495

[3] C. Casalegno, S. Russo, F. Sciarretta (2018). Numerical Analysis of a Masonry Panel Reinforced with Pultruded FRP Frames. Mech. Comp. Mater. 54(2):207-220

[4] A. Cecchi, S. Russo, F. Sciarretta (2017). Preliminary investigation on FRP profiles for the structural retrofit of masonry structures. Key Eng. Mater. 747:77-84. DOI: 10.4028/www.scientific.net/KEM.747.77

[5] https://l2mgc.cyu.fr/version-francaise/navigation/anr-postfire. Accessed 26/04/2021.

[6] M. V. Rossi (2003). Built heritage and its protection: 43°Corso ispettori antincendi - International firefighters' workshop. Fire service college, Moreton in Marsh, UK, 30th September - 2th October 2003. In Italian.

[7] A. Rafiee, M. Vinches, C. Bohatier (2008). Modelling and analysis of the Nîmes arena and the Arles aqueduct subjected to a seismic loading, using the Non-Smooth Contact Dynamics method. Eng. Struct. 30:3457-3467. DOI: 10.1016/j.engstruct.2008.05.018

[8] Th. Parent (2015). Méthodologie de Diagnostic de Structures Maçonnées Anciennes. PhD dissertation, University of Toulouse 3. In French. https://tel.archives-ouvertes.fr/tel-01403780

[9] C. Bukowski, V. Nuzzolese (2009). Performance-based fire protection of historical structures. Fire Technol. 45(1):23-42. DOI: 10.1007/s10694-008-0044-x

[10] Eurocode 6 – EN 1996-1-2, Design of Masonry Structures, Part 1-2: General Rules-Structural Fire Design (2005). European Committee for Standardization, Brussels, Belgium.

[11] NFPA 914 – Code for the protection of historic structures (2019). The National Fire Protection Association, Quincy, Massachusetts, USA

[12] M. El Boudani, N. Wilkie-Chancellier, L. Martinez, R. Hébert, O. Rolland, S. Forst, V. Vergès-Belmin, S. Serfaty (2015). Marble ageing characterization by acoustic waves. Phys. Proc. 70:222-226. DOI: 10.1016/j.phpro.2015.08.140

[13] J. D. Mertz, E. Colas, A. Ben Yahmed, R. Lenormand R (2016) Assessment of a non-destructive and portable mini permeameter based on a pulse decay flow applied to historic surfaces of porous materials. In: 13th International congress on the deterioration and conservation of stone, Paisley, Scotland 6-10th September 2016.

[14] S. McCabe, B. J. Smith, P. A. Warke (2007). Sandstone response to salt weathering following simulated fire damage: a comparison of the effects of furnace heating and fire. Earth Surf. Processes Landforms 32:1874-1883. DOI: 10.1002/esp.1503

[15]     V. Pachta, S. Triantafyllaki, M. Stefanidou (2018). Performance of lime-based mortars at elevated temperatures. Constr. Build. Mater. 189(11):576-684. DOI: 10.1016/j.conbuildmat.2018.09.027

[16]     P. Bamonte, P. G. Gambarova, F. Sciarretta (2020). Thermo-mechanical properties and stress-strain curves of ordinary cementitious mortars at elevated temperatures. Constr. Build. Mater. 267: 121027. DOI: 10.1016/j.conbuildmat.2020.121027

[17]     W. Jäger, T. Burkert (2001). The reconstruction of the Frauenkirche in Dresden. In: P. B. Lourenço, P. Roca (eds.); Historical Constructions, Guimarães, pp. 167-186.

[18]     S. J. Lawrence, N. Gnanakrishnan (1987). The fire resistance of masonry walls – An overview. In: A. C. T. Barton (ed.), First National Structural Engineering Conference, Institution of Engineers, Melbourne 26-28th August 1987

[19]     B. Chakrabarti, T. Yates, A. Lewry (1996). Effect of fire damage on natural stonework in buildings. Constr. Build. Mat. 10 (7) 539-544. DOI: 10.1016/0950-0618(95)00076-3

[20]     M. Vigroux, Influence de la microstructure et de la minéralogie sur l'endommagement mécanique des pierres de construction utilisées dans le patrimoine bâti sous l'effet de conditions environnementales sévères. PhD Thesis, Université de Cergy-Pontoise, 2020 (in French)

[21]     S. McCabe, B. J. Smith, P. A. Warke (2010). Exploitation of inherited weakness in fire-damaged building sandstone: the 'fatiguing' of 'shocked' stone. Eng. Geol. 115:217-225. DOI: 10.1016/j.enggeo.2009.06.003

[22]     F. Sciarretta, F. Antonelli, F. Peron, S. Caniglia (2018). Final outcomes on the multi-disciplinary long-term monitoring and preservation state investigation on the medieval external Façades of Palazzo Ducale in Venice, Italy. J. Civ. Struct. Health Monit. 8(11):111-133. DOI: 10.1007/s13349-017-0263-2

[23]     V. Pires, L. G. Rosa, A. Dionìsio (2014). Implications of exposure to high temperatures for stone cladding requirements of three Portuguese granites regarding the use of dowel–hole anchoring systems. Constr. Build. Mat. 64:440-450. DOI: 10.1016/j.conbuildmat.2014.03.035

[24]     W. S. Gonzalez Gomez, P. Quintana, A. May-Pat, F. Avilés, J. May-Crespo, J. J. Alvarado-Gil (2015). Thermal effects on the physical properties of limestones from the Yucatan peninsula. Int. J. Rock Mech. Min. Sci. 75:182-189. DOI: 10.1016/j.ijrmms.2014.12.010

[25]     P. D. Desai, R. A. Navarro, S. E. Hasan, C. Y. Ho, D. P. DeWitt, T. R. West (1974). Thermophysical properties of selected rocks. CINDAS Report 23

[26]     J. Sippel, S. Siegesmund, T. Weiss, K.-H. Nitsch, M. Korzen (2007). Decay of natural stones caused by fire damage. In: R. Přikryl and B. J. Smith (eds.), Building Stone Decay: From Diagnosis to Conservation. Geol. Soc. Spec. Publ. 271:139-151.

[27]     M. Hajpál, Á. Török (2004). Mineralogical and colour changes of quartz sandstones by heat. Env. Geol. 46:311–322. DOI: 10.1007/s00254-004-1034-z

[28]     R. N. Razafinjato, A.-L. Beaucour, R. Hébert, A. Noumowé, B. Ledésert, R. Bodet (2013). Thermal stability of different siliceous and calcareous aggregates subjected to high temperature. MATEC Web of Conf. 6:1-9. DOI: 10.1051/matecconf/20130607001

[29]     M. J. Heap, S. Mollo, S. Vinciguerra, Y. Lavallée, K. U. Hess, D. B. Dingwell, P. Baud, G. Iezzi (2013). Thermal weakening of the carbonate basement under Mt. Etna volcano (Italy): implications for volcano instability. J. Volc. Geotherm. Res. 250:42-60. DOI: 10.1016/j.jvolgeores.2012.10.004

[30]     F. Robert, H. Colina (2008). The influence of aggregates on the mechanical characteristics of concrete exposed to fire. Mag. Concr. Res. 61(5):311-321. DOI: 10.1680/macr.2007.00121

[31]     S. Gialanella, F. Girardi, G. Ischia, I. Lonardelli, M. Mattarelli, M. Montagna (2010). On the goethite to hematite phase transformation. J. Therm. Anal. Calorim. 102 (3) 867-873. DOI: 10.1007/s10973-010-0756-2

[32]     M. Hajpál (2002). Changes in sandstones of historical monuments exposed to fire or high temperature. Fire Technol. 38: 373–382.

[33]  Hager (2014). Sandstone colour change due to the high temperature exposure. Adv. Mat. Res. 875-877: 411-415. DOI: 10.4028/www.scientific.net/AMR.875-877.411

[34]  M. Hajpál (2010). Fire damaged stone structures in historical monuments. Laboratory analyses of changes in natural stones by heat effect, CIB publication: 164-173

[35]  A. Ozguven, Y. Ozcelik (2013). Effects of high temperature on physico-mechanical properties of Turkish natural building stones. Eng. Geol. 183: 127-136. DOI: 10.1016/j.enggeo.2014.10.006

[36]  S. Siegesmund and R. Snethlage (eds.) (2014). Stone in architecture. Properties, durability. Springer-Verlag: Berlin, 5th edition

[37]  G. Polyakova (2014). The main silica phases and some of their properties. In: J. W. P. Schmelzer (ed.), Glass – Selected properties and crystallization. Berlin: De Gruyter. DOI: 10.1515/9783110298581.197

[38]  S. P. Karunadasa, C. H. Manoratne, H. M. T. G. A. Pitawala, R. M. G. Rajapakse (2019). Thermal decomposition of calcium carbonate (calcite polymorph) as examined by in-situ high-temperature X-ray powder diffraction. J. Phys. Chem. Solid. 134:21-28. DOI: 10.1016/j.jpcs.2019.05.023

[39]  F. Homand-Etienne, R. Poupert (1989). Thermally induced microcracking in granites: characterization and analysis. Int. J. Rock Mech. Min. Sci. Geomech. Abstr. 26(2):125-124

[40]  A. V. Denisov, A. Sprince (2018). Analytical determination of thermal expansion of rocks and concrete aggregates. Mag. Civ. Eng. 4:151-170. DOI: 10.18720/MCE.80.14

[41]  R. D. Harvey (1967). Thermal expansion of certain Illinois limestones and dolomites. Urbana: Illinois State Geological Survey, Circular 415

[42]  A. Zeisig, S. Siegesmund, T. Weiss (2002). Thermal expansion and its control on the durability of marbles. Geol. Soc. Spec. Publ. 205:65-80

[43]  M. Vigroux, J. Eslami, A.-L. Beaucour, A. Bourgès, A. Noumowé (2021). High temperature behaviour of various natural building stones. Constr. Build. Mat. 272:121629. DOI: 10.1016/j.conbuildmat.2020.121629

[44]  X. F. Hu, T. T. Lie, G. M. Polomark, J. W. MacLaurin (1993). Thermal properties of building materials at elevated temperatures. National Research Council of Canada, internal report IRC-IR-643

[45]  E. Plevová, L. Vaculíková, A. Kožušníková, M. Ritz, G. Simha Martynková (2015). Thermal expansion behaviour of granites. J. Therm. Anal. Calorim. 123:1555-1561. DOI: 10.1007/s10973-015-4996-z

[46]  E. Plevová, L. Vaculíková, A. Kožušníková, T. Daněk, M. Pleva, M. Ritz, G. Simha Martynková (2011). Thermal study of sandstones from different Czech localities. J. Therm. Anal. Calorim. 103: 835-843. DOI: 10.1007/s10973-010-1129-6

[47]  V. Gräf, M. Jamek, A. Rohatsch, E. Tschegg (2013). Effects of thermal-heating cycle treatment on thermal expansion behavior of different building stones. Int. J. Rock Mech. Min. Sci. 64: 228–235. DOI: 10.1016/j.ijrmms.2013.08.007

[48]  R. Lopez-Doncel, W. Wedekind, A. Aguillón-Robles, R. Dohrmann, S. Molina-Maldonado, Th. Leiser, A. Wittenborn, S. Siegesmund (2018). Thermal expansion on volcanic tuff rocks used as building stones: examples from Mexico. Env. Earth Sci. 77: 338. DOI: 10.1007/s12665-018-7533-0

[49]  S. Siegesmund, K. Ullemeier, T. Weiss, E. K. Tschegg (2000). Physical weathering of marbles caused by anisotropic thermal expansion. Int. J. Earth Sci. 89: 170-182

[50]  V. Čermák, L. Rybach (1982). Thermal properties: Thermal conductivity and specific heat of minerals and rocks. In: G. Angeneister (ed.), Landolt-Bornstein numerical data and functional relationships in science and technology. New York: Springer

[51]  E. C. Robertson (1988). Thermal properties of rocks. US Department of the Interior Geological Survey, Open-file report 88-441

[52]    C. Clauser, E. Huenges (1995). Thermal conductivity of rocks and minerals. In: Th. J. Ahrens (ed.), Rock physics and phase relations: a handbook of physical constants. Washington: American Geophysical Union, pp. 105-126

[53]    T. Z. Harmathy (1983). Properties of building materials at elevated temperatures. National Research Council of Canada, Division of Building Research, paper 1080

[54]    S. Q. Miao, H. P. Li, G. Chen (2014). Temperature dependence of thermal diffusivity, specific heat capacity, and thermal conductivity for several types of rocks. J. Therm. Anal. Calorim. 115:1057-1063. DOI: 10.1007/s10973-013-3427-2

[55]    H.-D. Vosteen, R. Schellschmidt (2003). Influence of temperature on thermal conductivity, thermal capacity and thermal diffusivity for different types of rock. Phys Chem Earth 28:499-509

[56]    Q. Sun, Ch. Lü, L. Cao, W. Li, J. Geng, W. Zhang (2016). Thermal properties of sandstone after treatment at high temperature. Int. J. Rock Mech. Min Sci. 85:60-66. DOI: 10.1016/j.ijrmms.2016.03.006

[57]    M. Abdulagatov, S. N. Emirov, Z. Z. Abdulagatova, S. Y. Askerov (2006). Effect of Pressure and Temperature on the Thermal Conductivity of Rocks. J. Chem. Eng. Data 51:22-33. DOI: 10.1021/je050016a

[58]    M. G. Alishaev, I.M. Abdulagatov, Z.Z. Abdulagatova (2012). Effective thermal conductivity of fluid-saturated rocks – Experiment and modeling. Eng. Geol. 135-136:24-39. DOI: 10.1016/j.enggeo.2012.03.001

[59]    Eurocode 2 – EN 1992-1-2 (2004). Design of Concrete Structures, Part 1-2: General Rules-Structural Fire Design, 2004, European Committee for Standardization, Brussels, Belgium.

[60]    R. D. Dwivedi, R. K. Goel, V. V. R. Prasad, A. Sinha (2008). Thermo-mechanical properties of Indian and other granites. Int. J. Rock Mech. Min. Sci. 45:303-315. DOI: 10.1016/j.ijrmms.2007.05.008

[61]    Zh. Ch. Tang, M. Sun, J. Peng (2019). Influence of high temperature duration on physical, thermal and mechanical properties of a fine-grained marble. Appl. Therm. Eng. 156:34-50. DOI: 10.1016/j.applthermaleng.2019.04.039

[62]    Y.-L. Chen, J. Ni, W. Shao, R. Azzam (2012). Experimental study on the influence of temperature on the mechanical properties of granite under uni-axial compression and fatigue loading. Int. J. Rock Mech. Min. Sci. 56:62-66. DOI: 10.1016/j.ijrmms.2012.07.026

[63]    W. G. P. Kumari, P. G. Ranjith, M. S. A. Perera, B. K. Chen, I. M. Abdulagatov (2017). Temperature-dependent mechanical behaviour of Australian Strathbogie granite with different cooling treatments. Eng. Geol. 229:31-44. DOI: 10.1016/j.enggeo.2017.09.012

[64]    Y. Wang, B. Liu, H. Zhu, Ch. Yan, Zh. Li, Zh. Wang (2014). Thermophysical and mechanical properties of granite and its effects on borehole stability in high temperature and three-dimensional stress. Sci. World J., 650683. DOI: 10.1155/2014/650683

[65]    M. Y. Koca, G. Ozden, A. B. Yavuz, C. Kincal, T. Onargan, K. Kucuk (2006). Changes in the engineering properties of marble in fire-exposed columns. DOI: 10.1016/j.ijrmms.2005.09.007

[66]    Peng, G. Rong, M. Cai, M.-D. Yao, Ch.-B. Zhou (2016). Eng. Geol. 200:88-93. DOI: 10.1016/j.enggeo.2015.12.011

[67]    L.-Y. Zhang, X.-B. Mao, A.-H. Lu (2009). Experimental study on the mechanical properties of rocks at high temperature. Sci. China Ser. E: Technol. Sci. 52(3):641-646. DOI: 10.1007/s11431-009-0063-y

[68]    H. Su, H. Jing, Q. Yin, L. Yu (2018). Effect of thermal environment on the mechanical behaviors of building marble. Adv. Civ. Eng. 1326503. DOI: 10.1155/2018/1326503

[69]    S. Liu, J. Xu (2015). Analysis on damage mechanical characteristics of marble exposed to high temperature. Int. J. Damage Mech. 24(8):1180-1193. DOI: 10.1177/1056789515570507

[70]    P. G. Ranjith, D. R. Viete, B. J. Chen, M. S. A. Perera (2012). Transformation plasticity and the effect of temperature on the mechanical behaviour of Hawkesbury sandstone at atmospheric pressure. Eng. Geol. 151:120-127. DOI: 10.1016/j.enggeo.2012.09.007

[71]    Q. Rao, Zh. Wang, H. Xie, Q. Xie (2007). Experimental study of mechanical properties of sandstone at high temperature. J. Cent. South Univ. Technol. 14(1):478-483. DOI: 10.1007/s11771−007−0311−x

[72]    Y.-L. Zhang, Q. Sun, H. He, L. Cao, W. Zhang, B. Wang (2017). Pore characteristics and mechanical properties of sandstone under the influence of temperature. Appl. Therm. Eng. 113:537-543. DOI: 10.1016/j.applthermaleng.2016.11.061

[73]    S. Wei, Y. Yang, Ch. Su, S. R. Cardosh, H. Wang (2019). Experimental study of the effect of high temperature on the mechanical properties of coarse sandstone. Appl. Sci. 9:2424. DOI: 10.3390/app9122424

[74]    G. Wu, Y. Wang, G. Swift, J. Chen (2013). Laboratory investigation of the effects of temperature on the mechanical properties of sandstone. Geotech. Geol. Eng. 31:809-816. DOI: 10.1007/s10706-013-9614-x

[75]    T. D. Rathnaweera, P. G. Ranjith, X. Gu, M. S. A. Perera, W. G. P. Kumari, W. A. M. Wanniarachchi, A. Haque, J.C. Li (2018). Experimental investigation of thermomechanical behaviour of clay-rich sandstone at extreme temperatures followed by cooling treatments. Int. J. Rock Mech. Min. Sci. 107:208-223. DOI: 10.1016/j.ijrmms.2018.04.048

[76]    R. P. Borg, M. Hajpal, Á. Török (2013). The fire performance of limestone. Characterisation strategy for the fire performance of Maltese & Hungarian limestone. In: F. Wald, I. Burgess, K. Horova, T. Jana, J. Jirku (eds.), Application of Structural Fire Engineering, Prague, Czech Republic, 19-20th April 2013

[77]    W. Zhang, Q. Sun, Sh. Zhu, B. Wang (2017). Experimental study on mechanical and porous characteristics of limestone affected by high temperature. Appl. Therm. Eng. 110:356-362. DOI: 10.1016/j.applthermaleng.2016.08.194

[78]    G. Wu, D. Wang (2012). Mechanical and acoustic emission characteristics of limestone after high temperature. Adv. Mat. Res. 446-449:23-28. DOI: 10.4028/www.scientific.net/AMR.446-449.23

[79]    Q. Meng, M. Zhang, L. Han, H. Pu, Y. Chen (2019). Experimental research on the influence of loading rate on the mechanical properties of limestone in a high-temperature state. Bull. Eng. Geol. Env. 78:3479-3492. DOI: 10.1007/s10064-018-1332-4

[80]    R. K. Ibrahim, N. R. Ismail, H. M. Omar. Thermal effects on compressive strength of local limestone and claystone. ARO Sci. J. Koya Univ. 5(2):61-66. DOI: 10.14500/aro.10283

[81]    EN 12407. Natural stone test methods. Petrographic examination (2019)

[82]    Y.-L. Chen, S.-R. Wang, J. Ni, R. Azzam, T. M. Fernandez (2017). An experimental study of the mechanical properties of granite after high temperature exposure based on mineral characteristics. Eng. Geol. 220:234-242. DOI: 10.1016/j.enggeo.2017.02.010

[83]    X. Daoying (1995). Physico-mechanical property changes associated with mineral phase transition in granite. Chin. J. Geochem. 14(3):250-255

[84]    Z. K. Crosby, Ph. M. Gullett, S. A. Akers, S. S. Graham (2018). Characterization of the mechanical behavior of Salem limestone containing thermally-induced microcracks. Int. J. Rock Mech. Min. Sci. 101:54-62. DOI: 10.1016/j.ijrmms.2017.11.002

[85]    W. Yu, B. Liu, H. Zhu, Ch. Yan, Zh. Li, Zh. Wang (2014). Thermophysical and mechanical properties of granite and its effects on borehole stability in high temperature and three-dimensional stress. Sci. World J., Article ID 650683. DOI: 10.1155/2014/650683

[86]    Z. Papay, Á. Török (2017). Effect of thermal and freeze-thaw stress on the mechanical properties of porous limestone. Period. Polytech., Civ. Eng. 62(2):423-428. DOI: 10.3311/PPci.11100

[87]    Z. Kis, L. Szentmiklósi, F. Sciarretta (2017). Water uptake experiments of historic construction materials from Venice by neutron imaging and PGAI methods. Mater. Struct. 50:159. DOI: 10.1617/s11527-017-1004-z

[88]    M. I. Khan (2002). Factors affecting the thermal properties of concrete and applicability of its prediction models. Build. Env. 37: 607-614. DOI: 10.1016/S0360-1323(01)00061-0

[89]   A. S. Wagh (1993). Porosity dependence of thermal conductivity of ceramics and sedimentary rocks. J. Mater. Sci. 28: 3715-3721

[90]   D. Grgic, D. Amitrano (2009). Creep of a porous rock and associated acoustic emission under different hydrous conditions. J Geophys Res 114:B10201. DOI: doi.org/10.1029/2006JB004881

[91]   B. Vásárhelyi, P. Ván (2006). Influence of water content on the strength of rock. Eng. Geol. 84:70-74. DOI: 10.1016/j.enggeo.2005.11.011

[92]   E. Verstrynge, R. Adriaens, J. Elsen, K. Van Balen (2014). Multi-scale analysis on the influence of moisture on the mechanical behavior of ferruginous sandstone. Constr. Build. Mater. 54:78–90. DOI: 10.1016/j.conbuildmat.2013.12.024

[93]   Z. A. Erguler, R. Ulusay (2009). Water-induced variations in mechanical properties of clay-bearing rocks. Int. J. Rock Mech. Min. Sci. 46:355–370. DOI: 10.1016/j.ijrmms.2008.07.002

[94]   M. Kwasniewski, P. Rodriguez-Oitabén (2009) Effect of water on the deformability of rocks under uniaxial compression, in: I. Vrkljan (ed), Proc. Reg. Symp. of the International Society for Rock Mechanics (ISRM), Dubrovnik, Croatia, 29th-31st October 2009, pp. 271-276

[95]   U. Seipold, E. Huenges (1998). Thermal properties of gneisses and amphibolites high pressure and high temperature investigations of KTB-rock samples. Tectonophys. 291:173-178

# APPENDIX

**Table A1.** Granites ($\rho$ = density; $\phi$ porosity; $s_g$ = mean grain size)

| ID | Ref. | ID in ref. | source/colour | composition | $\rho$ (kg/m³) | $\phi$ (%) | $s_g$ (mm) |
|---|---|---|---|---|---|---|---|
| G1 | [25] | curve 82 | Uzbekistan | leucocratic granite | - | - | - |
| G2 | | curve 83 | Uzbekistan | biotite granite | - | - | - |
| G3 | | curve 84 | Uzbekistan | biotite granite | - | - | - |
| G4 | | curve 85 | Uzbekistan | pyromene-peridotite granite | - | - | - |
| G5 | [44] | - | Shandong province, China | - | - | - | - |
| G6 | [26] | KÖSS | Kösseine, Germany/bluish grey | plagioclase, K-feldspar, quartz, biotite, chlorite, masonite | - | 0.11 | - |
| G7 | [45] | 4573 | Pribram, Czech Republic | quartz 36%, orthoclase 42, plagioclase 14, biotite 5 | - | - | - |
| G8 | | 10256 | Sardinia, Italy | quartz 38%, orthoclase 37, plagioclase 15, biotite 5 | - | - | - |
| G9 | | 9696 | India | quartz 39%, orthoclase 48, plagioclase 10 | - | - | - |
| G10 | | 11780 | Liberec, Czech Republic | quartz 37%, orthoclase 40, plagioclase 18, biotite 2 | - | - | - |
| G11 | | 10109 | Zulova, Czech Republic | quartz 42%, orthoclase 35, plagioclase 15, biotite 7 | - | - | - |
| G12 | [50] | Sak73 | - | - | 2620 | - | - |
| G13 | | Moi68 | - | - | - | - | - |
| G14 | | Moi66 | - | - | - | - | - |
| G15 | | Hyn71 | - | - | - | - | - |
| G16 | [25] [50] | curve 2, Bir40 | Rockport, Massachusetts, USA | orthoclase 64% vol., quartz 28, amphibole 6, rest 2 | 2610 | - | 1.5-2 |
| G17 | | curve 3, Bir40 | Rockport, Massachusetts, USA | orthoclase 64% vol., quartz 28, amphibole 6, rest 2 | 2610 | - | 1.5-2 |
| G18 | | curve 4, Bir40 | Barre, Vermont, USA | albite 37% vol., quartz 26, orthoclase 25, biotite 9, muscovite 3 | 2650 | - | 1 |
| G19 | | curve 1, Bir40 | Westerly, Rhode Island, USA | albite 40% vol., orthoclase 33, quartz 19, biotite 6, rest 2 | 2640 | - | 0.5 |
| G20 | [25] | curve 7 | Rockville, Minnesota, USA | feldspar 56% vol., quartz 31, biotite 12, rest 1 | 2680 | - | coarse |

| G21 | | curve 8 | Rockville, Minnesota, USA | feldspar 56% vol., quartz 31, biotite 12, rest 1 | 2680 | - | coarse |
|---|---|---|---|---|---|---|---|
| G22 | [54] | - | Fuping, Hebei, China | oligoclase 70% vol., quartz 25, biotite 3, magnetite 1, microcline 1 | 2620 | 3.2 | coarse |
| G23 | [50] | Leo67 | - | - | - | - | - |
| G24 | | Win52 | - | - | - | - | - |
| G25 | [25] | curve 1 | Rockville, Minnesota, USA | microcline 34% vol., quartz 30, plagioclase 29, biotite 6, hornblend 1 | 2660 | - | 0.5-10.0 |
| G26 | | curve 15 | - | plagioclase 35% vol., quartz 25, biotite 5 | - | | |
| G27 | [51] | - | Rockville, Minnesota, USA | - | - | - | - |
| G28 | | - | charcoal grey | - | - | - | - |
| G29 | | - | - | - | - | - | - |
| G30 | | - | - | - | - | - | - |
| G31 | [60] | SbG | Salisbury | - | 2600 | | 0.5-2.0 |
| G32 | | WG | Westerly | quartz 29.3%, K-feldspar 31.4, plagioclase 31.3, biotite 3.8, muscovite 3, opaque 0.8 | 2600 | | |
| G33 | | - | charcoal | - | - | - | - |
| G34 | [62] | - | Ningbo, China / grey | quartz 28.3%, K-feldspar 30.5, plagioclase 31.1, mica 5.4 | - | - | - |
| G35[1] | [63] | - | Strathbogie, Australia | quartz 50% mass, plagioclase 16, biotite 15, K-feldspar 13 | 2703 | 1.16 | 0.2-0.5 |
| G36 | [60] | IG | India | quartz 39.5% vol., K-feldspar 48, plagioclase 10, biotite 1.5, amphibole 1 | 2590 | 0.8 | 2.6 |
| G37 | [39] | - | Remiremont, France | quartz 26% vol., K-feldspar 23, plagioclase 43, biotite 5, muscovite 3 | | | 1.7 |
| G38 | [82] | - | Nan'an City, Fujian Province, China / grey | plagioclase 45-50%, mica 25-30, quartz 15-20 | - | - | - |
| G39 | [85] | - | Mount Yan, North China | quartz, feldspar, hornblende | 2540 | - | - |
| G40 | [83] | - | Bolkezbek, Xinjiang, China | quartz 40%, orthoclase 30, plagioclase 20, biotite and muscovite 5 | - | - | - |
| G41 | [39] [60] | SG | Senones, France | quartz 14-20%, K-feldspar 34-45, plagioclase 30-35, biotite 5-10, amphibole 2-5 | - | - | - |
| vir | [55] | magmatic rocks | Tauern, Austria; basement of Adriatic plate | various igneous rocks | - | - | - |

[1]) a- hot, b- slow cooling, c- fast cooling

**Table A2.** Marbles (ρ = density; φ porosity; $s_g$ = mean grain size)

| ID | Ref. | ID in ref. | source/colour | composition | ρ (kg/m³) | φ (%) | $s_g$ (mm) |
|---|---|---|---|---|---|---|---|
| M1[1] | [25] | curves 46-51 | Crestmore, California, USA / sky blue | - | - | - | 2-3 |
| M2[2] | [25] | curves 23-25 | Yule Creek, Colorado, USA | - | - | - | - |
| M3 | [26] | C1 | Cava Ortensia, Italy | calcite, masonite <2% | - | 0.21 | - |
| M4 | | C2 | Cima di Gioia, Italy | pure calcite | - | 0.26 | - |
| M5 | | GTH | Thassos, Greece | dolomite, plagioclase | - | 0.54 | - |
| M6[3] | [25] [50] | curve 6 | Proctor, Vermont, USA | - | 2690 | ≈ 0 | - |
| M7 | [25] | curve 1 | Phillipsburg, Quebec, Canada / Missisquoi "white" | pure calcite with little organic matter | 2760 | - | - |
| M8 | | curve 3 | St. Marc des Carriers, Quebec, Canada / Deschambault "brown" | CaCO₃ 98% weight, organic matter | 2660 | - | - |
| M9 | | curve 4 | St. Albert, Ontario, Canada / Silvertone "black" | CaCO₃ 96% weight, organic matter | 2770 | - | - |
| M10 | [61] | - | Leiyang, Hunan, China | dolomite 93.05% vol., calcite 6.95% | - | 0.85 | 0.1-1.0 |

| ID | Ref. | ID in ref. | Source/colour | composition | ρ | φ | sg |
|---|---|---|---|---|---|---|---|
| M11 | [50] | Win52 | - | - | - | - | - |
| M12 | [25] | curve 1 | Knoxville, Tennessee, USA / Holston marble | calcite 99% vol., pyrite or magnetite <1 | 2680 | - | 0.2-1.5 |
| M13 | [51] | - | Tennessee, USA | - | - | - | - |
| M14 | | - | - | - | - | - | - |
| M15 | [65] | - | Izmir, Turkey | calcite 99%, quartz 1% | - | ≈0.3 | - |
| M16 | [35] | AW | Afyon, Turkey / white | crystalline calcite, recristallised thinney calcite veins and opaque minerals | 2716 | 0.2 | medium |
| M17 | | AG | Afyon Turkey / grey | calcite | 2716 | 0.1 | medium |
| M18 | | AT | Afyon, Turkey / tigerskin | crystalline calcite and small amount of opaque minerals and quartz | 2728 | 0.7 | coarse |
| M19 | | MM | Mugla Milas, Turkey | Calcite and small amount of muscovite, quartz and opaque minerals | 2725 | 0.7 | fine |
| M20 | [66] | - | Zhenping, Henan, China | dolomite, calcite and a small amount of biotite | 2700 | - | 3.0-4.0 |
| M21 | [67] | - | Xuzhou, China | - | - | - | - |
| M22 | [68] | - | Linyi, Shandong province, China / white | calcite, dolomite, quartz | 2830 | - | fine |
| M23 | [69] | - | Qinling, China | dolomite 90%, calcite 3, muscovite 3, amphibole 2, talc 1, quartz 1 | 2600 | - | - |
| vmr | [55] | - | Dolomites, Northern Alps | various metamorphic rocks | - | - | - |

(1) 1= first heat, 2= second heat; X= axis E-W, Z= axis N-S, Y= vertical axis

(2) second heat

(3) X= parallel to bedding, Y= perpendicular to bedding

**Table A3.** Sandstones (ρ = density; φ porosity; $s_g$ = mean grain size)

| ID | Ref. | ID in ref. | Source/colour | composition | ρ (kg/m³) | φ (%) | $s_g$ (mm) |
|---|---|---|---|---|---|---|---|
| S1 | [43] | GR | Rothbach, France | quartz, periclase, iron oxides | 2220 | 15.7 | 0.39 |
| S2 | [26] | ROWE | Wesernsandstein, Germany | quartz, plagioclase, k-feldspar, masonite, hematite, chlorite | - | 5.33 | fine |
| S3[(1)] | [25] | curves 1-3 | Penshaw sandstone, England | - | 2400 | 14.2 | - |
| S4[(2)] | | curves 7-8 | Chunking, China | quartz 68.33%, kaolinite 25.8, illite 2.98, sericite 2.15, pyrite 0.71, calcite 0.1 | 2629 | 3.0 | - |
| S5 | [46] | 10577 | Cerveny Kostelec | quartz, feldspar, dolomite, mica | - | - | 0.37 |
| S6 | | 7643 | Zamel, Czech Republic | quartz, chlorite, glauconite | - | - | 0.17 |
| S7 | | 7642 | Zamel, Czech Republic / white | quartz, chlorite, kaolinite | - | - | 0.23 |
| S8[(3)] | [25] | curves 1-2 | Allentown, Pennsylvania, USA | quartzitic sandstone | 2640 | ≈ 0 | 0.3 |
| S9 | [50] | Sak73 | - | - | 2620 | - | - |
| S10 | | Sak73 | - | - | 2600 | - | - |
| S11 | [56] | - | Linyi, Shandong province, China | quartz, feldspar, dolomite/ankerite, hematite/magnetite | 2410 | 7.8 | - |
| S12[(4)] | [25] | curves 4-5 | St. Peters, Minnesota, USA | quartz 98% vol., feldspar 1, kaolinite 0.5, illite 0.5 | - | 11.0 | - |
| S13[(4)] | | curves 6-7 | Teapot dome, Wyoming, USA | quartz 88% vol., kaolinite 7, illite 5 | - | 29.0 | - |
| S14[(4)] | | curves 8-9 | Berea, Ohio, USA | quartz 88% vol., kaolinite 10, illite 2 | - | 22.0 | - |
| S15 | [57] | - | Aktash, Dagestan, Russia | - | 2180 | 5.0 | moderate |
| S16[(5)] | [58] | sandstone-3 | Solonchak, Dagestan, Russia | - | 2180 | 13.0 | moderate |
| S17 | [51] | - | - | - | - | - | - |
| S18 | | - | - | - | - | - | - |
| S19 | [27] [32] | M | Maulbronner, Germany / reddish grey | quartz, chlorite, vermiculite, illite, hematite; cement type: clayey | - | 21.9 | fine |
| S20 | | Pf | Pfinztaler, Germany / greyish red | quartz, chlorite, illite, hematite; cement type: chlorite | - | 9.77 | medium |
| S21 | | Po | Postaer, Germany / off-white | quartz, kaolinite, illite, chlorite, smectite; cement type: siliceous | - | 22.79 | coarse |

| S22 | | B | Rohrschacher, Germany / grey | quartz, chlorite, glauconite, calcite, dolomite; cement type: calcareous | - | 2.54 | fine |
|---|---|---|---|---|---|---|---|
| S23 | | E | Ezusthegy, Hungary / white | quartz, kaolinite, chlorite; cement type: kaolinitic | - | 16.38 | fine |
| S24 | | R | Rezi, Humgary / greenish | quartz, kaolinite, chlorite, jarosite, barite; cement type: jarositic | - | 18.63 | medium |
| S25 | [70] | | Gosford, New South Wales | quartz 85% weight, kaolinite 7, illite/muscovite 3, goethite 2, smectite 2, anatase 1 | 2230 | 5.0 | medium-coarse |
| S26 | [71] | E | - | - | - | - | - |
| S27 | [72] | - | Linyi, Shandong province, China / dark red | - | - | 7.78 | - |
| S28 | [73] | A | - | - | 2346 | - | coarse |
| S29 | [67] | - | Xuzhou, China | - | - | - | - |
| S30 | [74] | - | Jiaozou, Henan province, China | quartz 73%, sericite 13%, calcite 5% | 2650 | - | 0.05-0.12 |
| S31 | [75] | - | Gosford, New South Wales | quartz 74%, kaolinite 12, siderite 7, barite 4, calcite 2, smectite <1, mica <1 | 2300 | 14.0 | 0.01-1.0 |
| vsr | [55] | - | Northern Alps, Dolomites, basement Adriatic plate | various sedimentary rocks | - | - | - |

[1] a= first heat, b= second heat, c= after use in a glass furnace

[2] a= no pre-heat, b= pre-heat at 1150°C

[3] X= parallel to bedding, Z= perpendicular to bedding

[4] a= heating, b= cooling

[5] 1= air saturated, 2= water saturated

**Table A4.** Limestones ($\rho$ = density; $\phi$ porosity; $s_g$ = mean grain size)

| ID | Ref. | ID in ref. | Source/colour | composition | $\rho$ (kg/m³) | $\phi$ (%) | $s_g$ (mm) |
|---|---|---|---|---|---|---|---|
| L1 | [43] | MA | Massangis, France | calcite, dolomite, quartz | 2391 | 11.2 | 0.63 |
| L2 | | LS | Lens, France | pure calcite | 2252 | 15.4 | 0.30 |
| L3 | | EUV | Euville, France | pure calcite | 2209 | 17.2 | 1.34 |
| L4 | | MI | Migné, France | pure calcite | 1949 | 26.8 | 0.07 |
| L5 | | MX | Saint-Maximin, France | calcite, quartz | 1791 | 29.7 | 0.31 |
| L6 | | SA | Savonnières, France | pure calcite | 1786 | 30.7 | 0.53 |
| L7[1] | [26] | EI | Eibelstadt, Germany | calcite, quartz, plagioclase | - | 4.64 | - |
| L8 | [25] | curve 1 | Rutland, Virginia, USA | crystalline | 2680 | 1.2 | - |
| L9 | | curve 4 | Batesville, Arkansas, USA | oolitic | 2660 | 1.8 | - |
| L10 | | curve 17 | Boulder County, Colorado, USA | breccia | 2800 | 18.8 | - |
| L11 | | curve 13 | Valcour Island, New York, USA / gray | - | 2710 | 0.7 | - |
| L12 | | curve 19 | Indiana, USA | - | - | - | - |
| L13 | [25] [50] | curve 5 Bir40 | Solenhofen, Bayern, Germany | - | 2605 | $\approx 0$ | 0.005 |
| L14[1] | [25] [50] | curve 6 Bir40 | Nazareth, Pennsylvania, USA | - | 2688 | $\approx 0$ | |
| L15 | [50] | Win52 | - | - | - | - | - |
| L16 | | Sak73 | - | - | 2700 | - | - |
| L17 | | Sak73 | - | - | 2750 | - | - |
| L18 | | Sak73 | - | - | 2600 | - | - |
| L19 | [25] | curve 1 | Indiana, USA | calcite 98,4% vol., quartz 1, hematite 0.6 | 2300 | - | fine |
| L20 | | curve 2 | Indiana, USA | calcite 98,4% vol., quartz 1, hematite 0.6 | 2300 | - | fine |
| L21 | | curve 3 | Queenston, Ontario, Canada / bluish-grey | MgCO₃ 22% weight, mixture of dolomite and calcite | 2670 | - | |
| L22 | | curve 4 | Longford Mills, Ontario, Canada / buff | MgCO₃ 30% weight, mixture of dolomite and calcite | 2560 | - | coarse |
| L23 | [57] [58] | - | Soltagasha, Dagestan, Russia | - | 2380 | 5.0 | - |
| L24 | [25] | curve 1 | Bedford, Indiana, USA | calcite 90% vol., organic 10 | 2320 | - | 0.25-1.0 |

| L25 | | curve 2 | Madhya Pradesh, India | - | - | - | - |
|---|---|---|---|---|---|---|---|
| L26 | [75] | - | Globigerina, Ta'Kandja, Malta | - | 1775 | - | - |
| L27 | [34] | freshwater | Süttő, Hungary / cream | cement: micritic calcite | - | - | fine |
| L28 | | compact | Tardos, Hungary / red | cement: micritic calcite | - | - | fine |
| L29 | | coarse | Sóskút, Hungary / yellowish white | cement: sparitic calcite | - | - | coarse |
| L30 | [35] | HP | Hazar pink | Sparitic limestone. Bioclast, calcite, organic | - | - | - |
| L31 | | DB | Daisy beige | Biosparitic limestone. Moderately crystalline calcite, opaque minerals | - | - | - |
| L32 | | SB | Sivrihisar beige | Sparitic limestone. Moderate crystalline calcite, recrystallized thin calcite veins, opaque minerals | - | - | - |
| L33 | | BB | Burdur beige | Sparitic limestone. Moderate crystalline calcite, recrystallized thin calcite veins, opaque minerals | - | - | - |
| L34 | [67] | - | Xuzhou, China | - | - | - | - |
| L35 | [77] | - | Linyi, Shandong province, China | - | 2710 | - | - |
| L36 | [78] | - | Jiaozuo, Henan province, China | calcite, dolomite, magnesite, other carbonate minerals | - | - | - |
| L37[2] | [79] | - | Xuzhou, Jiangsu province, China | calcite, dolomite, illite | 2720 | - | - |
| L38 | [80] | A | Fatha, Iran | - | 2670 | 0.75 | |
| L39 | [84] | - | Bedford, Indiana, USA | - | - | - | - |
| L40 | [86] | FR | Fertőrákos, Hungary | - | - | 24.6 | |
| L41 | | SM | Sóskút, Hungary | - | - | 24.4 | medium |
| L42 | | SF | Sóskút, Hungary | - | - | 35.6 | fine |
| vsr | [55] | - | Northern Alps, Dolomites, basement Adriatic plate | various sedimentary rocks | - | - | - |

[1] X= parallel to bedding, Z= perpendicular to bedding

[2] displacement rate 0.01 mm/s

**Table A5.** Testing parameters of researches on thermal expansion, conduction and specific heat

| ID | Ref. | Property | sample (shape, mm) | method, heating rate (°C/min) |
|---|---|---|---|---|
| G1-G4 | [25] | $\varepsilon_{th}$ | - | dilatometer |
| G5 | [44] | $\varepsilon_{th}$ | square prism 10-12 x 30-40 length | Theta dilatometer, 10°C/min |
| | | $\lambda$ | - | TC-31 thermal conductivimeter (Kyoto electronics) |
| | | $c_p$ | - | differential thermal analyser (DuPont), 10°C/min |
| G6 | [26] | $\varepsilon_{th}$ | cylinder $\varnothing$7x20 | dilatometer, 10°C/min |
| G7-G11 | [45] | $\varepsilon_{th}$ | cube 10 | thermal analyser + quartz probe, 30°C/min |
| G12-G15 | [50] | $\lambda$ | - | - |
| G16-G19 | [25, 50] | $\lambda$ | disc $\varnothing$38x6 | steady state absolute longitudinal method |
| G20-G21 | [25] | $\lambda$ | 127-152 thickness | non-steady line heat source method |
| G22 | [54] | $\lambda$ | | calculated from diffusivity, density and specific heat |
| | | $c_p$ | disc $\varnothing$12.7x2.5 | heat flux differential scanning calorimetry (Netsch-Gerätebau thermal analyser) |
| G23-G24 | [50] | $c_p$ | - | - |
| G25 | [25] | $c_p$ | - | drop copper block |
| G26 | [25] | $c_p$ | - | differential thermal analysis |
| G27-G30 | [51] | $c_p$ | - | - |
| G31-G33 | [60] | $c_p$ | - | - |
| vir | [55] | $\lambda$ | - | needle probe; divided bar device |
| | | $c_p$ | - | heat flux differential scanning calorimetry |
| M1 | [25] | $\varepsilon_{th}$ | - | dilatometer |
| M2 | [25] | $\varepsilon_{th}$ | - | dilatometer |
| M3-5 | [26] | $\varepsilon_{th}$ | cylinder $\varnothing$7x20 | dilatometer, 10°C/min |
| M6 | [25, 50] | $\lambda$ | disc $\varnothing$38x6 | steady state absolute longitudinal method |
| M7-9 | [25] | $\lambda$ | disc $\varnothing$20.3x2.5 | steady state absolute longitudinal method |
| M10 | [61] | $\lambda$, $c_p$ | - | - |

| | | | | |
|---|---|---|---|---|
| M11 | [50] | $c_p$ | - | - |
| M12 | [25] | $c_p$ | - | drop copper block |
| M13-M14 | [51] | $c_p$ | - | - |
| vmr | [55] | $\lambda$ | - | needle probe; divided bar device |
| | | $c_p$ | - | heat flux differential scanning calorimetry |
| S1 | [53] | $\varepsilon_{th}$ | cylinder $\varnothing$10x50 | dilatometer |
| | | $\lambda$, $c_p$ | couple of prisms 80x80x40 | Hotdisk TPL 1500 |
| S2 | [26] | $\varepsilon_{th}$ | cylinder $\varnothing$7x20 | dilatometer, 10°C/min |
| S3 | [25] | $\varepsilon_{th}$ | rod 200 length | dilatometer |
| S4 | [25] | $\varepsilon_{th}$ | cylinder $\varnothing$15x50 | dilatometer |
| S5-S7 | [46] | $\varepsilon_{th}$ | cube 10 | thermal analyser + quartz probe, 20°C/min |
| S8 | [25] | $\lambda$ | disc $\varnothing$38x64 | steady state absolute longitudinal method |
| S9-S10 | [50] | $\lambda$ | - | - |
| S11 | [56] | $\lambda$, $c_p$ | cylinder $\varnothing$50x30 | Hotdisk TPS |
| S12-S14 | [25] | $\lambda$ | cylinder $\varnothing$102x178 with axial hole $\varnothing$3.2x165 | line heat source |
| S15 | [57] | $\lambda$ | cylinder | steady-state absolute parallel-plate |
| S16 | [58] | $\lambda$ | cylinder | steady-state absolute parallel-plate |
| S17-S18 | [51] | $c_p$ | - | - |
| vsr | [55] | $\lambda$ | - | needle probe; divided bar device |
| | | $c_p$ | - | heat flux differential scanning calorimetry |
| L1-L6 | [43] | $\varepsilon_{th}$ | cylinder $\varnothing$10x50 | |
| | | $\lambda$, $c_p$ | couple of prisms 80x80x40 | Hotdisk TPL 1500 |
| L7 | [26] | $\varepsilon_{th}$ | cylinder $\varnothing$7x20 | dilatometer, 10°C/min |
| L8-L11 | [25] | $\varepsilon_{th}$ | - | dilatometer |
| L12 | [25] | $\varepsilon_{th}$ | rod of uniform section | dilatometer |
| L13-L14 | [25, 50] | $\lambda$ | disc $\varnothing$38x6 | steady state absolute longitudinal method |
| L15-L18 | [50] | $\lambda$ | - | - |
| L19-L20 | [25] | $\lambda$ | cylinder $\varnothing$91x457 | steady state radial absolute method |
| L21-L22 | [25] | $\lambda$ | disc $\varnothing$203x25 | steady state absolute longitudinal method |
| L23 | [57, 58] | $\lambda$ | cylinder | steady-state absolute parallel-plate |
| L24 | [25] | $c_p$ | - | drop copper block |
| L25 | [25] | $c_p$ | - | adiabatic calorimeter |

**Table A6.** Testing parameters of researches on residual mechanical properties

| ID(s) | Ref. | Method or standard | Sample (mm) | state | heating rate (°C/min) | duration at maximum temperature (h) | cooling regime | load, stress or displacement rate |
|---|---|---|---|---|---|---|---|---|
| G34 | [62] | recommendations of ISRM[1] | cylinder $\varnothing$40x80 | residual | 10 | 6 | closed oven | 0.5 MPa/s |
| G38 | [82] | | cylinder $\varnothing$50x100 | residual | 5 | 6 | closed oven | 0.5 kN/s |
| G35 | [63] | uniaxial compression | cylinder $\varnothing$22.5x45 | hot; residual | 5 | 2 | water; closed oven | 0.1 mm/min |
| G31-33, G36 | [60] | recommendations of ISRM[1] | cylinder $\varnothing$58x145 | hot | 1-2 | 5 | - | unspecified |
| G37 | [39] | uniaxial compression | cylinder $\varnothing$50x100 | hot | 0.8-1.7 | 5 | - | unspecified |
| G37, G41 | [39] | direct tension | cylinder $\varnothing$50x100 | residual | 0.8-1.7 | 5 | - | unspecified |
| G39 | [85] | uniaxial compression | cylinder $\varnothing$50x100 | hot | - | 2 | - | unspecified |
| M10 | [61] | uniaxial compression | cylinder $\varnothing$50x100 | residual | 5 | 0.5; 1; 2; 3; 4; 8 | out of oven | 0.5 kN/s |
| M15 | [65] | uniaxial compression | cylinder $\varnothing$50x100 | hot | variable | 3 | - | unspecified |
| M16-19, L30-33 | [35] | uniaxial compression | cylinder | residual | 5 | 1 | closed oven | unspecified |
| | | indirect tension | cylinder | residual | 5 | 1 | closed oven | unspecified |
| M20 | [66] | uniaxial compression | cylinder $\varnothing$50x100 | residual | 10 | 4 | out of oven | 0.075 mm/min |

| M21, S29, L34 | [67] | uniaxial compression | cylinder ⌀20x45 | hot | 120 | 2 | - | 0.004 mm/s |
|---|---|---|---|---|---|---|---|---|
| M22 | [68] | uniaxial compression | cylinder ⌀50x100 | residual | 5 | 2 | closed oven | 0.003 mm/s |
| M23 | [69] | recommendations of ISRM[1] | cylinder ⌀50x100 | residual | 10 | 2 | closed oven | 0.8 MPa/s |
| S1, L1-L6 | [43] | uniaxial compression NF EN 1926 | cylinder ⌀40x80 | residual | 4 | 1 | closed oven | 100 µm/min |
| | | indirect tension NF P 94-422 | cylinder ⌀40x40 | residual | 4 | 1 | closed oven | 1 kN/min |
| | | cyclic compression (*E* and v) | cylinder ⌀40x80 | residual | 4 | 1 | closed oven | 100 µm/min |
| L27-29 | [34] | uniaxial compression | cylinder ⌀40 | residual | variable | 6 | closed oven | unspecified |
| S25 | [70] | uniaxial compression ASTM D7012-07 | cylinder ⌀23x46 | hot | 5 | unspecified[2] | - | 0.1 mm/min |
| S26 | [71] | uniaxial compression | cube 50 | hot | 30 | 2 | - | 5 µm/s |
| | | Brazilian disc test | disc ⌀50x50 | hot | 30 | 2 | - | 5 µm/s |
| S27 | [72] | uniaxial compression | cylinder ⌀50x100 | residual | 5 | unspecified | unspecified | 500 N/s |
| S28 | [73] | uniaxial compression | cylinder ⌀50x100 | residual | 10 | 4 | closed oven | 0.02 mm/s |
| S30 | [74] | uniaxial compression | cylinder ⌀50x100 | residual | 5 | 2 | closed oven | unspecified |
| S31 | [75] | ASTM C-39 | cylinder ⌀36x76 | residual | 5 | 24 | water; closed oven | 0.1 mm/min |
| L26 | [76] | BS EN 1926 | cube 50 | hot | unspecified | 6 | - | unspecified |
| L36 | [78] | uniaxial compression | cylinder ⌀50x100 | residual | 5 | 2 | closed oven | unspecified |
| L37 | [79] | uniaxial compression | cylinder ⌀50x100 | residual | 10 | 4 | closed oven | 0.01 mm/s[3] |
| L38 | [80] | ASTM D7012 | cylinder ⌀75x140 | residual | none[4] | 2 | out of oven | unspecified |
| L39 | [84] | quasi-static uniaxial compression | cylinder ⌀50x110 | residual | variable | 5 | -1°C/min | variable[5] |
| L35 | [77] | uniaxial compression | cylinder ⌀50x100 | residual | 5 | 2 | -0.5°C/min | unspecified |
| L40-42 | [86] | indirect tension AFNOR P94-422 | cylinder ⌀50x25 | residual | unspecified | 2 | out of oven | unspecified |

[1] ISRM – International Society of Rock Mechanics
[2] duration as long as the compressive test
[3] value selected among different rates
[4] cold samples put into the hot furnace
[5] quasi-static tests

**Table A7.** Granites - mean values and 65% confidence intervals of properties

| Series | normalised property | T (°C) | mean value | superior 65-quantile | inferior 65-quantile |
|---|---|---|---|---|---|
| G1-G11 | $\alpha_T / \alpha$ | 100 | 1.46 | 1.89 | 1.03 |
| | | 200 | 1.00 | 1.00 | 1.00 |
| | | 300 | 1.81 | 2.47 | 1.16 |
| | | 400 | 2.28 | 2.69 | 1.88 |
| | | 500 | 1.80 | 2.25 | 1.36 |
| | | 550 | 3.97 | 4.15 | 3.78 |
| | | 575 | 10.29 | 12.12 | 8.46 |
| | | 600 | 8.21 | 9.37 | 7.05 |
| | | 700 | 3.54 | 4.53 | 2.55 |
| | | 750 | 7.71 | 10.23 | 5.19 |
| | | 900 | 2.57 | 2.80 | 2.35 |
| | | 975 | 2.39 | 3.07 | 1.72 |
| G5, G12, G13, G15-G21, vir | $\lambda_T / \lambda$ | 30 | 0.99 | 1.00 | 0.98 |
| | | 50 | 0.96 | 0.97 | 0.95 |
| | | 100 | 0.90 | 0.91 | 0.88 |

| | | 200 | 0.78 | 0.80 | 0.76 |
|---|---|---|---|---|---|
| | | 300 | 0.67 | 0.70 | 0.65 |
| | | 400 | 0.60 | 0.63 | 0.58 |
| | | 500 | 0.55 | 0.59 | 0.52 |
| | | 600 | 0.56 | 0.64 | 0.48 |
| G5, G24, G26, G29-G33, vir | $c_{p,T}$ / $c_p$ | 50 | 1.01 | 1.05 | 0.98 |
| | | 100 | 1.07 | 1.09 | 1.05 |
| | | 200 | 1.20 | 1.24 | 1.16 |
| | | 300 | 1.21 | 1.26 | 1.16 |
| | | 400 | 1.33 | 1.39 | 1.27 |
| | | 500 | 1.32 | 1.39 | 1.25 |
| | | 600 | 1.38 | 1.46 | 1.30 |
| | | 800 | 1.55 | 1.70 | 1.41 |
| G34, G35, G37, G38 | $f_{c,res,T}$ / $f_c$ | 200 | 1.06 | 1.14 | 0.98 |
| | | 400 | 0.85 | 0.89 | 0.81 |
| | | 600 | 0.40 | 0.41 | 0.38 |
| | | 800 | 0.25 | 0.33 | 0.17 |
| G35, G36, G39 | $f_{c,hot,T}$ / $f_c$ | 100 | 1.04 | 1.10 | 0.99 |
| G34, G35, G37, G38 | $E_{res,T}$ / $E$ | 200 | 0.87 | 0.95 | 0.80 |
| | | 400 | 0.71 | 0.87 | 0.56 |
| | | 600 | 0.45 | 0.49 | 0.40 |
| | | 800 | 0.06 | 0.40 | 0.04 |
| G35, G36, G40 | $E_{hot,T}$ / $E$ | 100 | 0.90 | 0.96 | 0.84 |
| G34, G35, G37, G38 | $\varepsilon_{c1,res,T}$ / $\varepsilon_{c1}$ | 200 | 1.30 | 1.48 | 1.12 |
| | | 400 | 1.40 | 1.55 | 1.25 |
| | | 600 | 1.61 | 1.70 | 1.51 |
| | | 800 | 2.00 | 2.18 | 1.82 |

**Table A8.** Marbles - mean values and 65% confidence intervals of properties

| Series | normalised property | T (°C) | mean value | superior 65-quantile | inferior 65-quantile |
|---|---|---|---|---|---|
| M1, M3-M5 | $\alpha_T$ / $\alpha$ | 200 | 1.19 | 1.47 | 0.91 |
| | | 300 | 2.00 | 2.16 | 1.84 |
| | | 400 | 2.15 | 2.39 | 1.91 |
| | | 500 | 2.21 | 2.54 | 1.87 |
| | | 600 | 2.21 | 2.31 | 2.11 |
| | | 700 | 2.35 | 2.44 | 2.27 |
| M6, M10, vmr | $\lambda_T$ / $\lambda$ | 200 | 0.80 | 0.89 | 0.70 |
| M10, M11, M14, vmr | $c_{p,T}$ / $c_p$ | 200 | 1.41 | 1.54 | 1.27 |
| | | 400 | 1.46 | 1.48 | 1.44 |
| M10, M16-M20, M22, M23 | $f_{c,res,T}$ / $f_c$ | 200 | 1.00 | 1.04 | 0.95 |
| | | 400 | 0.88 | 0.96 | 0.79 |
| | | 600 | 0.77 | 0.84 | 0.84 |
| | | 800 | 0.48 | 0.58 | 0.58 |
| | | 1000 | 0.23 | 0.29 | 0.29 |
| M10, M20, M22, M23 | $E_{res,T}$ / $E$ | 200 | 0.73 | 0.84 | 0.63 |
| | | 400 | 0.53 | 0.67 | 0.40 |
| | | 600 | 0.44 | 0.52 | 0.35 |
| M10, M20, M22, M23 | $\varepsilon_{c1,res,T}$ / $\varepsilon_{c1}$ | 200 | 1.43 | 1.46 | 1.40 |
| | | 400 | 1.86 | 2.03 | 1.70 |
| | | 600 | 2.46 | 2.73 | 2.20 |
| M16-M19 | $f_{t,T}$ / $f_t$ | 200 | 0.99 | 1.03 | 0.94 |
| | | 400 | 0.64 | 0.67 | 0.61 |
| | | 600 | 0.48 | 0.52 | 0.43 |
| | | 800 | 0.33 | 0.37 | 0.28 |
| | | 1000 | 0.04 | 0.06 | 0.02 |

**Table A9.** Sandstones - mean values and 65% confidence intervals of properties

| Series | normalised property | T (°C) | mean value | superior 65-quantile | inferior 65-quantile |
|---|---|---|---|---|---|
| S1-S7 | $\alpha_T$ / $\alpha$ | 200 | 1.03 | 1.05 | 1.00 |
| | | 400 | 1.97 | 2.20 | 1.74 |
| | | 550 | 3.72 | 4.08 | 3.36 |
| | | 575 | 9.42 | 10.68 | 8.17 |

| Series | normalised property | T (°C) | mean value | superior 65-quantile | inferior 65-quantile |
|---|---|---|---|---|---|
| | | 600 | 6.04 | 7.96 | 4.12 |
| | | 700 | 0.53 | 0.68 | 0.38 |
| | | 900 | 0.80 | 1.12 | 0.47 |
| | | 950 | 0.74 | 0.84 | 0.64 |
| S1, S8-S16, vsr | $\lambda_T / \lambda$ | 50 | 0.94 | 0.96 | 0.92 |
| | | 100 | 0.86 | 0.90 | 0.82 |
| | | 150 | 0,84 | 0.91 | 0.77 |
| | | 200 | 0,75 | 0.78 | 0.71 |
| | | 250 | 0.81 | 0.84 | 0.78 |
| | | 300 | 0.64 | 0.68 | 0.59 |
| | | 400 | 0.66 | 0.69 | 0.62 |
| | | 500 | 0,60 | 0.63 | 0.56 |
| | | 537 | 0,48 | 0.51 | 0.45 |
| | | 600 | 0.58 | 0.65 | 0.51 |
| S1, S11, S17, S18, vsr | $c_{p,T} / c_p$ | 200 | 1.33 | 1.45 | 1.21 |
| | | 250 | 1.31 | 1.39 | 1.23 |
| | | 300 | 1.39 | 1.47 | 1.30 |
| | | 400 | 1.49 | 1.55 | 1.42 |
| | | 800 | 1.91 | 2.12 | 1.71 |
| S1, S19-S24, S27, S28, S30, S31 | $f_{c,res,T} / f_c$ | 100 | 1.06 | 1.13 | 0.99 |
| | | 150 | 1.04 | 1.10 | 0.98 |
| | | 200 | 1.02 | 1.04 | 0.99 |
| | | 300 | 1.10 | 1.15 | 1.04 |
| | | 400 | 1.08 | 1.14 | 1.02 |
| | | 450 | 1.21 | 1.31 | 1.11 |
| | | 600 | 0.99 | 1.06 | 0.92 |
| | | 750 | 0.89 | 1.05 | 0.73 |
| | | 800 | 0.90 | 0.95 | 0.84 |
| | | 900 | 0.82 | 0.98 | 0.67 |
| S25, S26, S29, S31 | $f_{c,hot,T} / f_c$ | 200 | 0.90 | 1.15 | 0.65 |
| | | 400 | 1.01 | 1.37 | 0.65 |
| | | 600 | 1.10 | 1.49 | 0.71 |
| | | 800 | 0.90 | 1.27 | 0.52 |
| S27, S28, S30, S31 | $E_{res,T} / E$ | 200 | 0.83 | 0.95 | 0.70 |
| | | 400 | 0.81 | 1.01 | 0.61 |
| | | 600 | 0.45 | 0.60 | 0.30 |
| | | 800 | 0.61 | 0.75 | 0.48 |
| S25, S26, S29, S31 | $E_{hot,T} / E$ | 200 | 0.99 | 1.10 | 0.87 |
| | | 400 | 1.09 | 1.21 | 0.96 |
| | | 600 | 0.97 | 1.03 | 0.92 |
| | | 800 | 0.68 | 0.71 | 0.65 |
| S27, S28, S30, S31 | $\varepsilon_{c1,res,T} / \varepsilon_{c1}$ | 100 | 1.04 | 1.08 | 1.01 |
| | | 200 | 1.12 | 1.22 | 1.02 |
| | | 400 | 1.11 | 1.16 | 1.06 |
| | | 600 | 1.89 | 2.01 | 1.78 |
| S25, S29, S31 | $\varepsilon_{c1,hot,T} / \varepsilon_{c1}$ | 200 | 1.09 | 1.33 | 0.85 |
| | | 400 | 1.20 | 1.38 | 1.02 |
| | | 600 | 1.45 | 1.76 | 1.13 |
| | | 800 | 1.76 | 2.20 | 1.32 |
| S27, S30, S31 | $\nu_{res,T} / \nu$ | 200 | 0.99 | 1.28 | 0.69 |
| | | 400 | 1.08 | 1.47 | 0.68 |
| | | 600 | 0.44 | 0.61 | 0.27 |

**Table A10.** Limestones - mean values and 65% confidence intervals of properties

| Series | normalised property | T (°C) | mean value | superior 65-quantile | inferior 65-quantile |
|---|---|---|---|---|---|
| L1-L12 | $\alpha_T / \alpha$ | 100 | 0.95 | 1.05 | 0.85 |
| | | 400 | 2.16 | 2.30 | 2.01 |
| | | 600 | 3.58 | 4.02 | 3.15 |
| | | 800 | 3.11 | 4.08 | 2.14 |
| | | 900 | -0.70 | 1.54 | -2.94 |
| | | 1000 | -10.28 | -7.32 | -13.25 |
| L1-L6, L13-18, L23, vsr | $\lambda_T / \lambda$ | 50 | 0.92 | 0.93 | 0.90 |
| | | 100 | 0.84 | 0.86 | 0.82 |
| | | 150 | 0.83 | 0.84 | 0.82 |

| | | | | | |
|---|---|---|---|---|---|
| | | 200 | 0.73 | 0.75 | 0.71 |
| | | 250 | 0.72 | 0.73 | 0.70 |
| | | 300 | 0.61 | 0.63 | 0.58 |
| | | 400 | 0.51 | 0.55 | 0.48 |
| | | 500 | 0.55 | 0.57 | 0.53 |
| | | 550 | 0.56 | 0.57 | 0.54 |
| | | 600 | 0.53 | 0.55 | 0.51 |
| L1-L6, vsr | $c_{p,T} / c_p$ | 150 | 1.22 | 1.24 | 1.20 |
| | | 200 | 1.27 | 1.29 | 1.25 |
| | | 250 | 1.32 | 1.34 | 1.30 |
| | | 300 | 1.40 | 1.42 | 1.37 |
| | | 500 | 1.73 | 1.78 | 1.68 |
| | | 550 | 1.97 | 2.05 | 1.89 |
| | | 600 | 2.21 | 2.34 | 2.08 |
| L1-L6, L27-L33, L35-L38 | $f_{c,res,T} / f_c$ | 150 | 0.95 | 1.07 | 0.83 |
| | | 200 | 0.94 | 098 | 0.90 |
| | | 300 | 0.90 | 0.99 | 0.81 |
| | | 400 | 0.89 | 0.94 | 0.84 |
| | | 450 | 0.86 | 0.97 | 0.75 |
| | | 600 | 0.68 | 0.72 | 0.63 |
| | | 800 | 0.45 | 0.50 | 0.40 |
| | | 1000 | 0.18 | 0.19 | 0.17 |
| L35-L37, L39 | $E_{res,T} / E$ | 200 | 0.70 | 0.76 | 0.63 |
| | | 400 | 0.40 | 0.44 | 0.36 |
| | | 500 | 0.29 | 0.34 | 0,24 |
| | | 600 | 0.26 | 0.33 | 0.18 |
| | | 800 | 0.15 | 0.20 | 0.11 |
| L35-L37 | $\varepsilon_{c1,res,T} / \varepsilon_{c1}$ | 200 | 1.29 | 1.54 | 1.04 |
| | | 400 | 1.64 | 1.84 | 1.43 |
| | | 600 | 2.29 | 2.30 | 2.27 |
| L1-L6, L30-L33, L40-L42 | $f_{t,T} / f_t$ | 200 | 0.97 | 0.99 | 0.95 |
| | | 300 | 0.97 | 0.99 | 0.95 |
| | | 400 | 0.83 | 0.91 | 0.76 |
| | | 600 | 0.63 | 0.69 | 0.57 |
| | | 800 | 0.52 | 0.59 | 0.44 |
| | | 1000 | 0.29 | 0.34 | 0.24 |